Synthesis of a new pyrimidine-based sorbent for indium(III) removal from aqueous solutions – Application to ore leachate

Mohammed Hamza, Abd Allh M. Abd El-Hamid, Eric Guibal, Adel A.H. Abdel-Rahman, Rania El Araby

Synthesis of a new pyrimidine-based sorbent for indium(III) removal from aqueous solutions – Application to ore leachate

Mohammed F. Hamza [a,b,1], Abd Allh M. Abd El-Hamid [b], Eric Guibal [c,*], Adel A.H. Abdel-Rahman [d], Rania El Araby [d]

[a] School of Nuclear Science and Technology, University of South China, Heng Yang 421001, China
[b] Nuclear Materials Authority, POB 530, El-Maadi, Cairo, Egypt
[c] Polymers Composites and Hybrids (PCH), IMT Mines Ales, Alès, France
[d] Chemistry Department, Faculty of Science, Menoufia University, Shebin El-Kom, 32511, Egypt

ARTICLE INFO

Keywords:
Synthesis of a new sorbent (as micro-particles) by formaldehyde polycondensation of thiobarbituric acid and thiocarbazide
Poorly porous material (low specific surface area) with high density of N-groups (and presence of S-reactive sites) for In(III) sorption in weakly acidic solution (pH 4)
Exothermic indium sorption decreasing from 1.87 to 1.24 mmol In g^{-1} when temperature increases from room temperature to 50°C, while sorption isotherm are fitted by Langmuir and Sips equations
Equilibrium is reached in 20–30 min, and kinetic profile is fitted by pseudo-first order rate equation (although the resistance to intraparticle diffusion cannot be neglected)
Indium readily desorbed from saturated sorbent using 0.3 M HCl solutions
The eluent weakly affects the sorption performance at recycling of the sorbent that reveals high stable
The sorbent is highly selective for trivalent cations against mono- or divalent cations with a relative preference for indium against other tested trivalent cations (both in synthetic solutions and acidic leachate of ore sample)

ABSTRACT

A new sorbent (TcTDG, pyrimidine derivative, with high content of N-based reactive groups and S-based sites) was successfully synthesized by the polycondensation of thiocarbazide and 2-thiobarbituric acid through reaction with formaldehyde. The material is characterized by FTIR, SEM and SEM-EDX analyses, titration, elemental analysis, BET, and TGA. After interacting with In(III), the FTIR spectrum of TcTDG shows the modification of the environment of N- and S-based reactive groups. The sorption of In(III) is first studied in synthetic solutions with TcTDG micro-particles through the evaluation of pH effect (optimum at pH 4), the uptake kinetics (equilibrium achieved in 20–30 min), the sorption isotherms and the selectivity properties from equimolar solution of different metal ions. The sorption capacity significantly decreases when increasing the temperature from 15 to 50 °C: In(III) sorption onto TcTDG is exothermic. Maximum sorption capacity at room temperature and at pH 4 reaches up to 1.87 mmol In g^{-1}; the isotherm is equally fitted by the Langmuir and the Sips equations. Indium is fully eluted from metal-loaded sorbent using 0.3 M HCl solution (equilibrium reached in 20–30 min). The pseudo-first order rate equation fits well experimental kinetic profile; although the resistance to intraparticle diffusion plays a significant role in the control of In(III) sorption. The sorbent is highly stable at recycling: the FTIR spectrum is restored after five cycles and desorption remains complete along the cycles; after five re-uses, the sorption efficiency decreases by less than 4%. The study is extended to more complex solutions: first, with multi-component synthetic equimolar solutions before investigating the application of TcTDG to metal recovery from acidic leachate of ore sample (from Eastern Central Desert, Egypt). The sorbent shows a marked preference for In(III) at pH 4 against mono-, di- and tri-valent metal ions in synthetic solutions, the preference is also appreciable but the selectivity coefficient ($SC_{In/metal}$) is weaker for rare metals (between 3 and 6, *vs.* 10–35 for other metal ions). In the case of acidic leachate, the pH control to 4 leads to substantial precipitation of huge amounts of iron and the co-precipitation of other metal ions. The sorption capacity for In(III) (and Ga(III)) is significantly reduced by the complexity of the effluents; although the sorbent maintains a preference for these trivalent metal ions. The new sorbent shows promising sorption properties, although complementary investigation is required for optimizing the practical application of this material (conditioning, larger number of recycling steps, etc.).

1. Introduction

Indium is a strategic metal mainly used in the fabrication of indium tin oxide that enters in the manufacturing of key materials such as liquid crystal display screens (LCDs, such as touch screens, flat screen TVs), and solar panels [1]. As a salt (under the form nitride, phosphide, or antimonide) it behaves as a semiconductor in transistor and chips. Indium metal is used for coating technical glasses (mirror finish, protective film, etc.) [1]. These wide uses combined with its relatively weak abundance on earth crust make the extraction, valorization and

* Corresponding author at: IMT - Mines Alès, PCH, 6 avenue de Clavières, F-30319 ALES CEDEX, France.
E-mail addresses: m-fouda21@usc.edu.cn (M.F. Hamza), eric.guibal@mines-ales.fr (E. Guibal).
[1] Co-corresponding author at: Nuclear Materials Authority, POB 530, El-Maadi, Cairo, Egypt.

recycling of the metal a strategic issue, which motivates the design of new sorbents and new strategies for its recovery from marginal ores and secondary sources (including waste materials) [2,3]. The Clarke number of indium is lower than 0.1 ppm much lower than other rare metals such as gallium (with Clarke number close to 19 ppm). Therefore, usually indium is not directly extracted from mining resources but as a by-product of zinc refineries. As an example, indium and zinc are coherently associated in vein deposits that contain precious metals, such as the Toyoha mine in Japan [4]. Recently, Pradhan et al. [5] reported that the annual production of indium from secondary resources exceeds the mining production. European Commission ranks indium among the critical raw materials taking into account its position into the frame "Supply Risk *vs.* Economic Importance" [6].

The valorization of marginal ores and secondary sources (waste electric and electronic equipment) usually proceeds through a first acidic leaching step [7–10]. The recovery of indium from liquid phases issued from both leachates and zinc refineries [11] may involve solvent extraction [12–17], supported liquid membranes and supports [18–21], or sorption [7,22].

A large number of sorbents have been reported for their capacity to bind In(III). Mineral sorbents including aluminosilicates [23], reduction-mediated sorption (using zero-valent iron, [24]), composite organic/inorganic sorbents [25–28] showed interesting removal properties for In(III), as well as carbon-based materials such as carbon nanotubes [29] or graphene oxide [30]. However, most of the investigated sorbents concern ion-exchange, chelating resins bearing carboxylate [31], iminodiacetate [7,32–34], phosphonic or aminophosphonic resins [35], N-methylglucamine groups [7], or impregnated resins [22,36]. Non-commercial sorbents have been also designed by grafting functional groups onto polymers [37] or biopolymers [38–41], compounding different supports [42], or coating inert support with reactive biopolymer layer [25].

The strong reactivity of thiourea for binding metal ions has been frequently used for the desorption of metal ions [43]. However, this reactivity was also taken into consideration for designing functionalized sorbents [44–48]. The bi-functionalization of sorbent reveals an interesting strategy for designing new sorbents for the removal of metal ions [49–54]. The presence of different functional groups leads to the modulation of acid-base properties, hydrophilic behavior, and coordination geometry, which, in turn, affect the pH range for efficient sorption, the uptake kinetics (mass transfer), the sorption capacity (density of sorption sites), and sorbent selectivity for target metals [51,55–57]. The analysis of literature motivated the synthesis of the new sorbent developed in this study (TcTDG). The sorbent (bearing amine and sulfur groups) is obtained by the reaction of 2-thiobarbituric acid (TPD, synthesized from diethyl malonate and thiourea precursors) with thiocarbazide (synthesized from carbon disulfide and hydrazine precursors) [58], followed by polycondensation (TcTDG), using formaldehyde. The dense and close co-existence of -C = S groups and -N–H groups offers high reactivity to the material; in addition, the condensation can contribute to steric arrangement that may orientate the selectivity of the sorbent.

After characterization of the physicochemical properties of the sorbent (through SEM, SEM-EDX, textural, TGA, FTIR, elemental analysis and titration for pH_{PZC} determination), the sorption properties of TcTDG are investigated for In(III) recovery from aqueous solutions. The pH effect (at two temperatures) is carried out, before investigating the effect of metal concentration on uptake kinetics; sorption isotherms are compared at four temperatures to qualify the thermodynamic characteristics of In(III) sorption. Metal desorption and sorbent recycling are investigated along five cycles of re-use. Prior to investigate the application of Tc-TDG to the treatment of ore leachates, the selectivity of the sorbent is carried out at different pH values from multi-component equimolar solutions. The main objective of this work focuses on the evaluation of the potential of this bifunctional (N- and S-donor reactive groups) sorbent for the removal of In(III) strategic element from dilute complex solutions; answering the following question. Is it meaningful processing to the cyclization of maleic anhydride with readily synthesized 2-thiobarbituric acid and polymerizing this intermediary reagent with thiocarbazide by formaldehyde?

2. Materials and methods

2.1. Materials

Carbon disulfide (>99.0%), hydrazine hydrate (50–60%), diethyl malonate (99.0%), sodium ethoxide (>95%), thiourea (>99.0%), glutaraldehyde (25.0%; w/w), formaldehyde (37.0%), acetone (≥99.5%), glacial acetic acid, indium (III) sulfate (anhydrous; ≥98.0%), gallium (III) nitrate (99.99%)*, calcium chloride (>97.0%)*, hydrochloric acid (37%), and sodium perchlorate (≥98.0) were supplied by Sigma Aldrich (Merck KGa, Darmstadt, Germany). Iron (III) sulfate (97.0%)*, sodium chloride (>99.0%)*, aluminum chloride (99.1%)*, magnesium chloride (95.0%)*, and zinc chloride (98.0%)* were purchased from Guangdong Guanghua Sci-Tech Co., Ltd (Guangdong, China). Cerium nitrate (>99.0%) * was supplied by the National Engineering Research Centre of Rare Earth Metallurgy and Functional Materials Co., Ltd (Baotou, China).

Note: * corresponds to salts used in selectivity experiments.

2.2. Synthesis of sorbent

First, thiocarbazide was synthesized by progressively reacting hydrazine hydrate (10 g, 50–60%, w/w, 100 mmol) with carbon disulfide (7.6 g, 100 mmol) in a round bottom flask disposed in an ice bath (Scheme 1a). The dropwise addition took place for a total duration of 90 min. The resulting mixture was stirred for 2 h to produce a white precipitate of thiocarbazide (12.4 g, meaning quantitative reaction) after drying the precipitate at 40 °C. The structure was elucidated by FTIR and mass spectra (see Figures S1-S2).

Thiobarbituric acid (i.e., 2-thioxodihydropyrimidine-4,6(1H,5H)-dione) was prepared by reaction of sodium ethoxide solution 50 % (200 mL) (heated at 80 ± 5 °C) with thiourea (6.4 g, 100 mmol) and diethyle malonate (15 g, 100 mmol) in round bottom flask equipped with condenser (Scheme 1b). The mixture was maintained under stirring and reflux (70–80 °C) for 10 h before being poured onto ice bath (600 mL flask), and acidified with 0.05 M HCl solution to reach pH close to 3.5–4. The mixture was kept stirring overnight. The product was filtered, dried and recrystallized using ethanol to give 2-thioxodihydropyrimidine-4,6(1H,5H)-dione (TDP, mp: above 300 °C), as a white powder with high conversion (the yield reaches 17.7 g, meaning a grafting close to 83%, on weight basis). The chemical characterization of TDP is reported in Figures S3-S5).

The sorbent (TcTDG) was synthesized by the reaction of thiocarbazide (11 g, ≈104 mmol) with TDP (7 g, 48.6 mmol) (previously dissolved in 150 mL absolute ethanol pre-acidified with 2 mL of concentrated H_2SO_4) (Scheme 1c). The reaction was maintained under reflux for 8 h at 80 °C. After filtration, the precipitate was washed-up and dried (i.e., 15 g). This intermediary product (10 g) was dissolved in demineralized water (50 mL) acidified with 1.5 mL acetic acid before adding formaldehyde (8.5 mL, 37%, w/w). The reactor was heated at 85 °C under reflux for 8 h, before pouring the solution into 200 mL of demineralized water containing an excess amount of 10 % glutaraldehyde (w/w). The agitation was maintained overnight; the final product

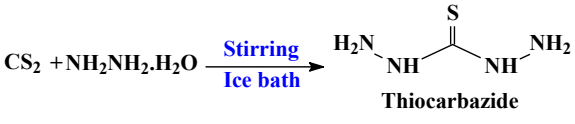

Scheme 1a. Synthesis of thiocarbazide (MW: 106.15 g mol^{-1}).

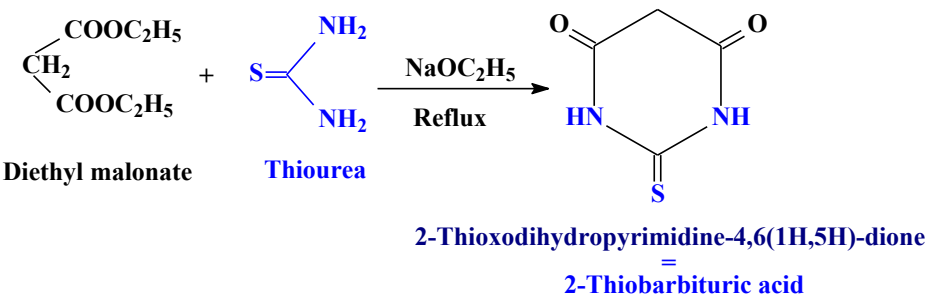

Scheme 1b. Synthesis route of 2-thiobarbituric acid (TDP, 2-thioxodihydropyrimidine-4,6(1H,5H)-dione; MW: 144.15 g mol^{-1}).

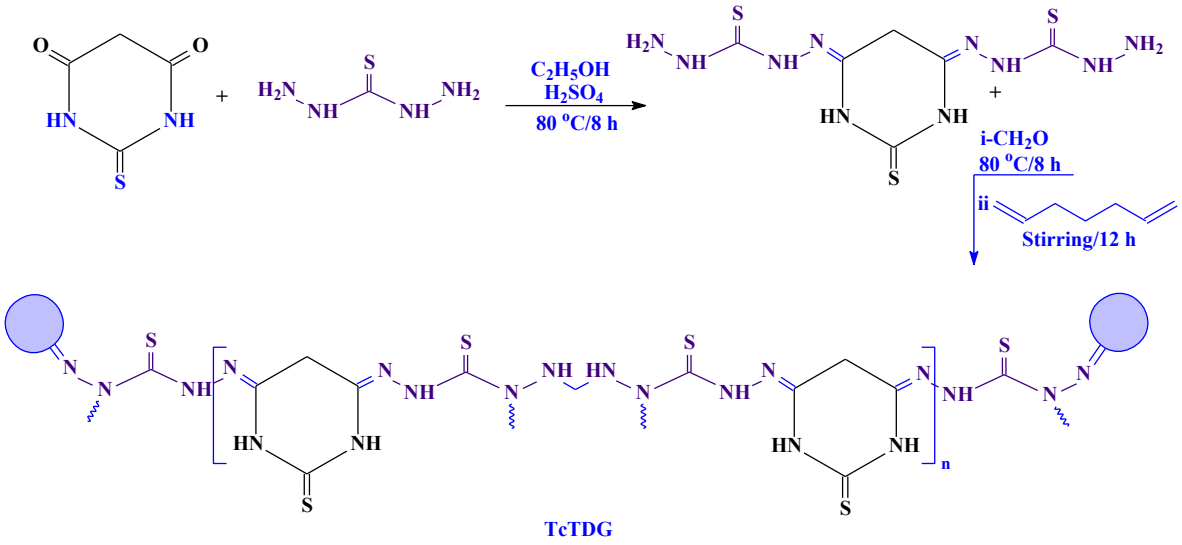

Scheme 1c. Synthesis route of TcTDG sorbent.

was filtered, washed-up with acetone and dried at 50 °C to produce TcTDG sorbent (12 g). The yield is close to 90%. The material was grinded and sieved; the fraction below 20 μm (Sieve N° 625) was retained.

2.3. Characterization of materials

The porosity and surface area of the sorbent were analyzed through N_2 adsorption–desorption isotherms using TriStar II surface area and porosity analyzer (Micromeritics, Norcross, GA, USA) operated at 77 K. The BET method was used for the determination of specific surface area while the BJH method was processed for analyzing the porous characteristics. The sorbent sample was first swept under N_2 gas (for 4 h at 110 °C). Morphological surface study was performed through SEM analysis (before and after loading) by Phenom ProX-SEM (Thermo Fisher Scientific, Eindhoven, Netherlands). The chemical composition of the prepared sorbent was semi-quantitatively determined by energy dispersive X-ray (EDX) analysis. FT-IR analysis was performed on dry samples after grinding and mixing with dried KBr to prepare KBr pellets. FTIR spectra were collected on IR-Tracer100 spectrometer (Shimadzu, Tokyo, Japan). The pH of the zero charge (pH_{pzc}) was determined by titration using the pH-drift method [59]. The thermal decomposition of TcTDG sorbent was analyzed by thermogravimetry under N_2 atmosphere with STA-449-F3 Jupiter thermal analyzer (Netzsch Gerätebau HGmbh, Selb, Germany); the temperature ramp was set at 10 °C min^{-1}.

The adjustment of the pH of the solution and the recording of equilibrium pH values (after sorption) were operated on a S220-Seven pH-ionometer (Mettler-Toledo, Shanghai, China). The metal ion concentration was measured using a ICP-AES (inductively coupled plasma atomic emission spectrometer, 7510 ICP-AES Shimadzu, Tokyo, Japan). The mass spectra were recorded by electron ionization technique (at 70 eV) with a 5988 GS-MS mass spectrometer (Hewlett-Packard, Palo Alto, CA, USA). NMR spectra were collected using DMSO-d_6, at room temperature (tetramethylsilane was used as the internal standard) with a Mercury-300 NMR spectrometer (Varian, Inc., Palo Alto, CA, USA). The elemental analysis of sorbent was processed using a Vario-EL cube (Elementar Analysensysteme GmbH, Langenselbold; Germany).

2.4. Sorption procedures and modeling

The sorption properties of TcTDG for In(III) have been performed in batch system. A fixed amount of sorbent (m, g) was mixed for fixed contact time (t, min) with a volume of solution (V, L) containing the metal ion (at concentration C_0, mmol L^{-1}) and fixed initial pH value (i.e., pH_0), at room temperature (T: 21 ± 1 °C), under agitation (v: 210 rpm). The sorbent dose, SD, is calculated as m/V. After given contact times (t for uptake kinetics, or after 24–48 h for equilibrium tests), a sample of suspension was collected and filtrated (membrane filter: 1.2-μm pore size), before being analyzed by ICP-AES. The pH was not controlled during sorption test but the final pH (i.e., pH_{eq}) was systematically recorded. The sorption capacity (q, mmol In g^{-1}) was deduced from mass balance equation: $q=(C_0-C_{eq}) \times V/m$. The distribution ratio (i.e., D, L g^{-1}) is obtained from $D = q_{eq}/C_{eq}$. The selectivity coefficient for the sorption of In(III) in the presence of competitor metal (Me) (i.e., $SC_{In/Me}$) is defined by:

$$SC_{In/Me} = \frac{D_{In}}{D_{Me}} = \frac{q_{eq,In} \times C_{eq,Me}}{C_{eq,In} \times q_{eq,Me}} \quad (1)$$

Desorption tests were also performed in batch system. For kinetics, the metal-loaded samples (collected at the end of kinetic experiments) were mixed with the eluent (0.3 M HCl solution) using a SD of 2 g L^{-1}, at room temperature and for 2 h. The mass balance equation was used for evaluating the desorption yield (%). For the study of sorbent recycling, sorption and desorption steps were performed using the same procedure and a washing step (with demineralized water) was systematically intercalated between each individual sorption and desorption steps. The complete experimental parameters are reported in the caption of relevant figures. Experiments were duplicated and the figures show average values with error bars.

Conventional models were used for fitting experimental profiles. Uptake kinetics were fitted with: (a) the pseudo-first order rate (PFORE [60]), (b) the pseudo-second order rate (PSORE [60]), and (c) the resistance to intraparticle diffusion (RIDE, via the Crank's equation [61]). The quality of the fit was analyzed by the determination coefficient (R^2) and the Akaike information criterion (AIC). Parameters were obtained by non-linear regression analysis (using Mathematica® facilities). The Langmuir, Freundlich, Sips [62], Temkin [63], and Dubinin-Radushkevich [64] equations were used for the simualtion of sorption isotherms. The formal non-linear forms of these equations are summarized in Tables S1 and S2 (see Section A, Supplementary Information).

2.5. Application to mining effluent

The sorbent has been tested for the recovery of valuable metals (including indium) in complex effluents. A mining ore collected in the Central Eastern Desert (Egypt) (Figure S17) was first leached using hydrochloric acid. The composition of the ore is summarized in Table S5. The detailed procedure is described in the Supplementary Information (Section D). The leachate was analyzed and the composition is reported in Table S6 (for target metals). The presence of a huge concentration of Fe(III) causes a strong precipitation of iron and co-precipitation of other metals when adjusting the pH. The percentage of metal precipitation was systematically quantified and taken into account for the calculation of effective sorption capacities (at fixed pH values). The contact time was set to 10 h, while the sorbent dose was 5 g L^{-1}.

3. Results and discussion

3.1. Synthesis and characterization of intermediary reagents

The different steps in the synthesis are confirmed by detailed analysis of intermediary products (see Section B in Supplementary Information). The Taguchi method is used for synthesizing one of the precursors (thiocarbazide) [65]. The mass spectrum of thiocarbazide shows molecular ion peak *m/z* 106.5 (representing 3.73%) and its fragmentation compounds for CH_6N_4S (Figure S2).

The synthesis of TDP (2-thiobarbituric acid) by reaction of diethyl malonate with thiourea is confirmed by the FTIR spectrum (see below), which shows similar profile than the spectrum deeply described by Mendez [66]. Most of the bands are characteristics of the solid form of 2-thiobarbituric acid; though some additional bands may be associated with tautomeric forms [67]. ^{1}H and ^{13}C NMR patterns are reported in Figure S4 [67,68]. ^{1}H NMR and ^{13}C NMR spectra of 2-thiobarbituric acid show characteristic signals at $\delta = 3.912$ (s, 2H, CH_2 alkane), 7.034 (2brs, 2H, 2NH), 12.039 (d, H, SH), and $\delta = 39.523$ (CH_2), 164.032 (2C = O), 183.877 (C = S) ppm, respectively. On the other hand, mass spectrum of TDP shows molecular ion peak *m/z* at 144.91 (8.83%) and its fragmentation for ($C_4H_4N_2O_2S$), (Figure S5).

Figure S6 reports the FTIR spectra of precursors (thiourea, thiocarbazide, and TDP) together with the spectrum of TcTDG. The sorbent is characterized by a broad band at 3428 cm^{-1}, which is assigned to $\nu_{N\text{-}H}$ vibration (probably associated with $\nu_{O\text{-}H}$ vibration, due to water absorption). Amine and imine groups are also identified by a broad band centered at 1620 cm^{-1} (covering $\delta_{N\text{-}H}$ and $\nu_{C=H}$). The small band at 2582 cm^{-1} can be correlated with $\nu_{S\text{-}H}$ vibration (evidence of tautomerization of C=S group from thiobarbituric acid moiety, appearing as enol form). The bands at 1082 and 1053 cm^{-1} may be correlated to N-C=S vibrations; these bands also appear in thiocarbazide. Rao and Venkataraghavan [69] reviewed the literature and concluded that the extreme variations (in the range 850–1570 cm^{-1}) in the assignment of the C=S stretching vibration is due to vibrational coupling effects. The contribution of C=S group is weakened by the relatively low fraction of these functional groups compared with the amine and imine groups in the final product.

The comparison of the FTIR spectrum of TcTDG with those of the precursors (thiourea, [70,71]; thiocarbazide, [72]; thiobarbituric acid, [73–75]) shows huge differences including: (a) appearance and disappearance of signals, and (b) substantial shifts in the wavenumbers (Figure S6). These variations allow following the synthesis of the material. However, the interpretation is made complex by some tautomeric effects. For example, Tellez-Soto et al. [73] deeply discussed the impact of tautomerization on the FTIR spectrum of thiobarbituric acid (enol and keto tautomeric forms). These mechanisms may strongly change the wavenumber of the vibrations of relevant reactive groups. The comparison of thiourea and thiobarbituric acid (TDP) spectra shows the grafting of diethyl malonate (with the appearance of carbonyl groups) in the range 1750–1500 cm^{-1}: (a) shift of the peak at 1615 to 1627 cm^{-1}, and (b) appearance of the bands at 1712 cm^{-1} ($\nu_{C=O}$) and 1567 cm^{-1} (N–H vibrations affected by environment modification). This is also confirmed by the appearance of a series of peaks in the range 1400–1100 cm^{-1} (environment of amine groups and coordination with carbonyl groups). The band at 805 cm^{-1} can be partially explained by the contribution of the TDP ring [73], or the out-of-plane $\delta_{C5\text{-}H}$ [66]. The changes observed at low wavenumber (below 700 cm^{-1}) can be assigned to the modification of the environment of C-N, C-N-C bond vibrations. The reaction of TDP with thiocarbazide also dramatically changes the spectrum. This may be due to the modification of the environment of N-based groups, the introduction of additional S-groups, and the effect of cyclization (ring formation). This is marked by:

(a) The disappearance of the bands at 3102 and 2872 cm^{-1};

(b) The replacement of the carbonyl-associated bands (at 1712 cm^{-1} and neighbors) by a broad band (centered at 1620 cm^{-1});

(c) The disappearance of the bands in the range 1500–1250 cm^{-1} (replaced by a broad band at 1383 cm^{-1}), and.

(d) The reinforcement of the band at 827 cm^{-1}.

3.2. Sorbent characterization

3.2.1. Morphology (SEM) and semi-quantitative EDX analysis

In Figure S7, the grinded fraction of the sorbent (sieved below 20 μm) appears as irregular in size and shape. The distribution of particle size was not determined but most of these particles (in weight) are 5 ± 1 μm (with significant fractions at 1–2 μm and some large particles around 10 μm). The shapes of sorbent particles can be qualified as ovoid massive appearance with irregularities (in surface morphology). The EDX analysis provides a semi-quantitative determination of the major elements present at the surface of sorbent particles. The high contents of nitrogen and sulfur elements confirm the efficient synthesis of the new sorbent (though the cyclization of precursors, rich in amine and sulfur groups). The presence of O element may be explained by partial hydration of the sorbent and/or the incomplete conversion of thiobarbituric acid (TDP, incomplete reaction with thiocarbazide).

3.2.2. Textural properties – N_2 sorption/desorption isotherms

The sorbent is poorly porous as shown in Figure S8 (duplicate analyses). The specific surface area is negligible (S_{BET} ≈0.23–0.63 m^2 g^{-1}). The poor specific surface area may explain the discrepancies appearing in the desorption branch of the N_2 sorption/desorption isotherms. These curves are simply convex and follow the typical Type III profiles according the IUPAC classification [76] (Figure S9a). This kind of profile is

usually associated with non-porous or macroporous solids. This is consistent with the limited porous volume (around 0.0029–0.0013 $cm^3 g^{-1}$). The hysteresis loop corresponds to H3 type: this mode is found in different systems such as non-rigid aggregates of plate-like particles (like in clay-based material); however, herein this is probably due to macroporous network, which is not completely filled with pore condensate [76]. The pore widths are significantly different when calculated from sorption and desorption branches (i.e., 319 Å and 203 Å, respectively for the first set, and 245–254 Å for the second set). This order of magnitude corresponds to mesoporous structure (according to the IUPAC classification: micropore less than 20 Å< mesopore less than 500 Å< macropore), apparently in contradiction with the analysis of the shape of N_2 isotherms. Figure S9b shows the distribution of pore size (diameter): the curve displays a maximum in the range 118–225 Å; however, a broad tail can be reported with sizes of several hundreds of Å. This means that a significant fraction of the porosity is constituted of macropores.

3.2.3. *Thermogravimetric analysis*

The thermodegradation profile of TcTDG is illustrated by weight loss curve and DTG plot (Figure S10). At 800 °C, the material is almost completely degraded: the residue does not exceed 8.2%. The degradation occurs in three main transitions:

(a) Below 194.2 °C, the loss (i.e., ≈19.7%) corresponds to water release;

(b) In the range 194.1–311.6 °C, the sorbent loses ≈33.8%; this is assigned to the depolymerization of TcTDG (probably completed with the degradation of ending amine groups [77]); and.

(c) Above 311.5 °C (up to 800 °C), the degradation of polymer chain (charring) associated with the progressive degradation of the char (above 550 °C).

These degradation steps can be correlated to the negative peaks observed on DTG curve: a shoulder at around 150 °C, followed by three marked peaks at 288.15 °C, 312.15 °C and 492.75 °C; the small peak at 614.35 °C deals with the final char degradation step.

3.2.4. *FTIR spectrophotometry – Sorbent interactions with In(III)*

The sorption of In(III) is operated at pH 4 (see below, Section 3.3.1.); this means that under these conditions, the pH control may affect the protonation of some reactive groups hold on the sorbent (see Section 3.2.5.). Therefore, it is important comparing not only the FTIR spectra of sorbent before and after In(III) sorption, but also with the spectrum of the sorbent conditioned at the pH of sorption study to be able to isolate the respective contributions of sorbent protonation and the proper interaction of In(III) ions with the reactive groups of the sorbent. Fig. 1 compares the spectra of TcTDG, TcTDG (at pH 4), and In(III)-loaded TcTDG (at the same pH). The broad band at 3428 cm^{-1} (convolution of $\nu_{N\text{-}H}$ and $\nu_{O\text{-}H}$ bands) is weakly shifted toward lower wavenumber when the polymer is conditioned at pH 4, and even more after binding In (III) (following the sequence: 3428 → 3424 → 3402 cm^{-1}): amine groups are involved in metal binding. Tiwari et al. [78] reported the significant shift of the $\nu_{N\text{-}H}$ after metal complexation using a Schiff-base derivative of thiobarbituric acid ligand. The small doublet bands at 2582 cm^{-1} (assigned to $\nu_{S\text{-}H}$ vibration) are changed in a single band at much lower wavenumber (i.e., 2538 cm^{-1}; double band at 2588 cm^{-1} for pH-controlled sorbent): sulfur-based reactive groups are also concerned by metal binding. After conditioning the sorbent at pH 4, the band at 1620 cm^{-1} (amine vibration) is enlarged with a shoulder at ≈1712 cm^{-1}; however, this modification disappears with In(III) binding, and the only change consists of a shift of the band to higher wavenumber (i.e., up to 1636 cm^{-1}). The band at 1053 cm^{-1} (assigned to asymmetric $\nu_{N\text{-}C=S}$) is shifted toward 1034 cm^{-1}. The poorly resolved band at 552 cm^{-1} disappears, while a new band appears at 679 cm^{-1}. The tautomerization effects change the effective form of the reactive groups and then their reactivity [79]. Therefore, the FTIR characterization is difficult for precisely establishing the active forms. However, the FTIR spectra demonstrate that uptake of In(III) involve N- and S-based reactive groups.

The spectrum of the sorbent after five cycles of In(III) sorption and desorption is also reported in Fig. 1. The comparison of this spectrum with that of the starting material shows that the sorbent is restored to its original state. There are only limited shifts in the relevant wavenumbers. The material shows good stability when submitted to successive sorption (at pH 4) and desorption (acidic solutions). This is consistent with the stability in sorption properties (see Section 3.3.6.).

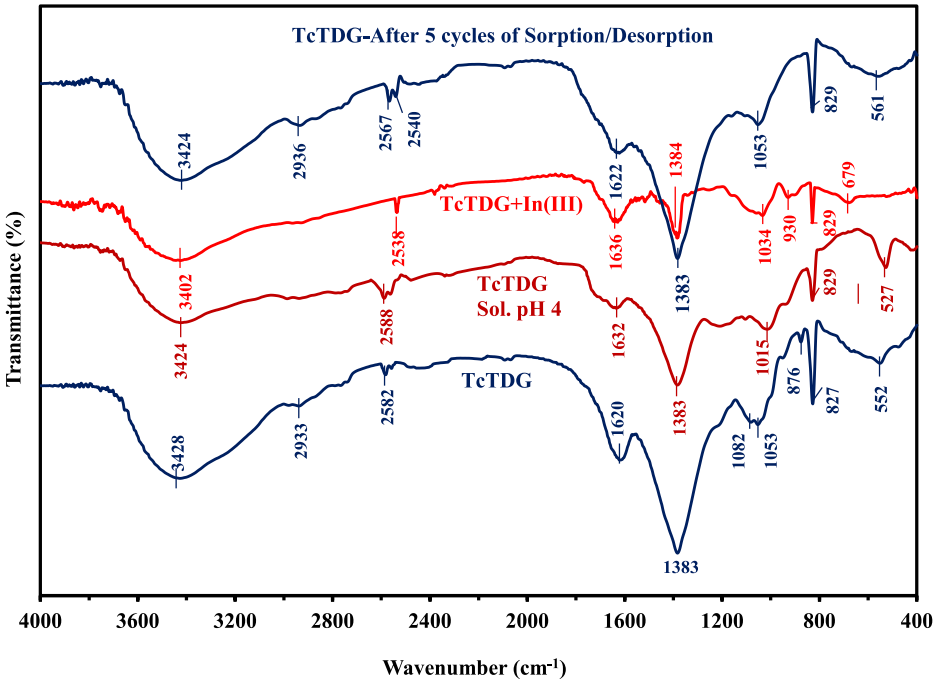

Fig. 1. FTIR spectra of TcTDG sorbent at different steps of use (pristine, after conditioning at pH 4, after In(III) sorption, and after five cycles of sorption/desorption).

3.2.5. Elemental analysis and pH_{PZC}

The elemental analysis shows the high density of both N-bearing and S-bearing groups (i.e., 24.6 ± 1.75 mmol N g^{-1} and 3.30 ± 0.47 mmol S g^{-1}, respectively) (Table S3). This is another proof of the successful synthesis procedure. The presence of O element (0.75 mmol O g^{-1}) is associated with either the hydration of the polymer (H_2O absorption) or the incomplete substitution of thiocarbazide onto thiobarbituric during the chemical grafting. It is noteworthy that the analyzed molar ratio N/S is close to 9.2, far above the expected molar ratio suggested by the hypothetical structure appearing in Sch. 1. This may confirm that the actual conversion is not fully achieved (incomplete substitution and/or reaction) or that the polymerization involves other reactive groups.

The pH-drift method allowed evaluating the pH of zero-charge (pH_{PZC}) (Figure S11). The concentration of the background salt (herein NaCl) slightly influences the pH_{PZC} value: from 5.59 to 5.78, when increasing salt concentration from 0.1 M to 1 M. Below pH 5.7, the sorbent is positively charged: the protonation of reactive groups progressively decreases with increasing the pH. The deprotonation improves the capacity of the sorbent to bind metal cations. Above pH 5.6, the overall charge of TcTDG is negative; conditions supposed to be more favorable for cation binding.

3.3. Indium sorption

3.3.1. Effect of pH

The pH may affect metal sorption through different effects associated with the chemistry of the metal (through speciation) and the protonation/deprotonation of reactive groups of the sorbent. Fig. 2 shows the pH-edge curves for In(III) sorption using TcTDG for 2 metal concentrations and two different temperatures. The four curves show the same trends:

(a) Weak sorption at acid pH (i.e., ≈1) q_{eq} below 0.25 mmol In g^{-1},
(b) Little increase in sorption at pH 2, followed by an inflexion,
(c) Steeper increase up to pH_{eq} ≈4.2, and.
(d) Progressive decrease above pH 4.5.

In acidic solutions, the strong protonation of reactive groups limits their availability for binding In(III). With pH increase, the progressive deprotonation enhances metal sorption. In addition, the tautomerization effect is favored by less acidic conditions. Figure S12a shows the speciation diagram of In(III) under the experimental conditions selected for pH study. At low pH, a small fraction of indium is present as anionic $In(SO_4)_2^-$ species, which can bind to protonated amine groups; this can explain that the sorption is not negligible even at pH 1. Above pH 4, free In^{3+} species becomes minority being replaced with hydrolyzed species with lower charge (neutral hydrolyzed indium becomes majority at pH higher than 4.5) [80]. Based on the pH_{PZC} value (i.e., ≈5.7) the sorbent remains protonated in this pH region. The sorption of indium may proceed under the control of competition effect (at low pH, with weak binding of anionic species), the ion exchange of cationic species with protonated amine groups, and the direct complexation of indium species with sulfide or sulfhydryl groups (at intermediary pH) (by analogy with the aqueous geochemistry of In(III), [81]). In Figure S12b, the log_{10} plot of the distribution ratio *vs.* pH_{eq} is characterized by an inversion of the slope around pH_{eq} 4 (which corresponds to the optimum pH condition for maximum sorption of indium, Fig. 2). This inversion is accompanied by a decrease in the slope: +0.4/0.5 at pH below 4 and −0.15/-0.32 at pH above 4. The pH 4-frontier can be correlated to the speciation diagram of the metal (Figure S12a): neutral hydrolyzed $In(OH)_{3,aq}$ begins to appear in the solution. At pH below 4, highly cationic species (i.e., free In^{3+} and $In(OH)^{2+}$) predominate, while above pH 4 neutral species (i.e., $In(OH)_{3,aq}$) and less-charged cationic species (i.e., $In(OH)_2^+$) become progressively predominant in the solution. The slope (close to 0.5) in acid region may be associated to a stoichiometric ratio for ion exchange close to 2 sorption sites per bound metal (as divalent cation). At milder pH, the predominance of species having less affinity for sorption sites (in terms of charge and steric hindrance) causes the decrease in sorption capacities and the change in the slope of the distribution coefficient plots. The binding of hydrolyzed species leads to the consumption of OH^- moieties leading to a relative pH decrease (while slightly increasing in acidic region, Figure S13).

It is noteworthy that the increase of the temperature from 21 °C to 50 °C involves a significant decrease of the sorption capacity (from 1.71 to 1.21 mmol In g^{-1}, at the highest metal concentration test): the sorption is exothermic.

The pH variation was systematically monitored during sorption tests (Figure S13): the pH remains stable in most cases. The largest variation occurs for the experiments performed at the highest concentration and at T: 50 °C. In this case, the equilibrium pH tends to progressively decrease above pH 4; reaching for pH_0 7 a value as low as 5.88 (only 6.72–6.84 for the other experimental conditions). The pH decrease is due to the release of protons and/or the binding of hydrolyzed indium species; though the strong effect observed at T: 50 °C cannot be easily explained.

The highest sorption capacities being obtained at pH 4 and the possible occurrence of hydrolysis (including precipitation) at higher pH values, lead to select pH 4 for further studies.

3.3.2. Uptake kinetics

The uptake kinetics at two initial concentrations are reported in Fig. 3. The equilibrium is reached in 20 min at the highest concentration

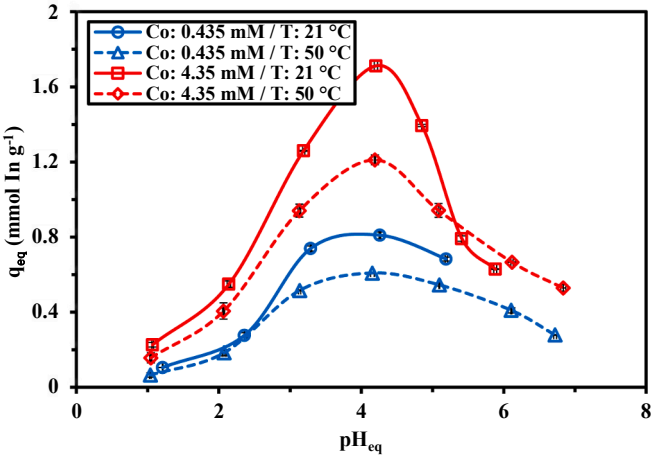

Fig. 2. Effect of pH on In(III) sorption capacity at two initial concentrations (C_0: 0.882 and 4.35 mmol In L^{-1}) and two temperatures (T: 21 ± 1 and 50 ± 1 °C) (Sorbent dose, SD: 0.667 g L^{-1}; v: 210 rpm; time: 48 h).

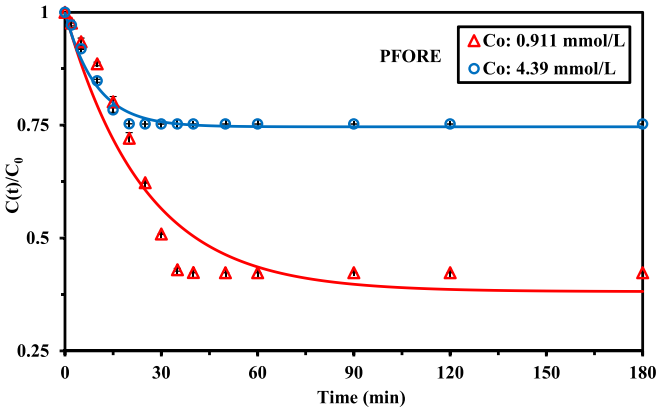

Fig. 3. In(III) uptake kinetics for two initial concentrations at pH_0 4 – Modeling with the Pseudo-first order rate equation (C_0: 0.911 and 4.39 mmol In L^{-1}; SD: 0.6 g L^{-1}; T: 21 ± 1 °C; v: 210 rpm).

(i.e., 4.39 mmol In L^{-1}), and 40 min at the lowest metal concentration (i.e., 0.9100 mmol In L^{-1}). This equilibrium time is consistent with the results reported by Van Roosendael [20] for indium recovery using supported ionic liquid phase, little faster than the equilibrium required in the case of functionalized composite [82], alginate-sulfonate-silica [42] or carbon nanotube [29]. The uptake kinetics can be controlled by mechanisms of resistance to diffusion (including bulk, film, and intraparticle diffusion). With a stirring speed of 210 rpm, the resistance to bulk diffusion is negligible. The resistance to film diffusion is usually taking a crucial part in the control of mass transfer in the first minutes of contact. Fig. 3 shows that the curves almost overlap within the first 15 min of contact: the metal concentration does not significantly affect the resistance to film diffusion expressed in the first contact phase. The two curves diverges more significantly in the next step, after 20 min of contact. In the case of high metal concentration, the strong concentration gradient allows rapidly saturating the reactive groups at the surface of the sorbent (and within the internal layers because of the thin particles; i.e., 5 ± 1 μm). On the opposite hand, at the lowest concentration, the weaker gradient requires a longer contact time to reach the equilibrium. In the case of In(III) uptake using chitosan and chitin, Franco et al. [83] observed that the mass transfer was controlled by the resistance to film diffusion. Alguacil et al. [29] concluded the same with carbon nanotubes.

In addition to the mechanisms of resistance to diffusion, the proper reaction rate may be also active in controlling the uptake kinetics. By analogy with chemical rate of homogeneous reactions, the pseudo-first order (PFORE) and the pseudo-second order rate (PSORE) equations may be used to fit the decay curves of concentrations (See Table S1). Three models were tested for fitting experimental profiles (PFORE, PSORE, and resistance to intraparticle diffusion (RIDE), as Crank equation). Table 1 compares the parameters of the models and the statistical criteria for In(III) uptake kinetics at C_0: 0.911 and 4.39 mmol In L^{-1}. The Akaike Information Criterion (AIC) is significantly different between two models when $|\Delta AIC| > 2$. Both R^2 and AIC values show that the PFORE model is more appropriate for fitting experimental profiles. In addition, PFORE shows sorption capacity at equilibrium ($q_{eq,1}$) closer from experimental value ($q_{eq,exp}$) than the PSORE: the equilibrium sorption capacity is overestimated by less than 7.3% (overestimation up to 14–30% for PSORE). In Fig. 2, the solid lines represent the PFORE fits of experimental profiles, while the fitting of the other models is shown in Figure S14. Hubbe et al. [84] reminded the conditions to be respected for the interpretation of kinetic profiles as chemical sorption. One of the major conditions (the quasi invariability of solute concentration) in the solution is not respected here for discussing the mechanism based on simple mathematical fit. The apparent rate coefficient (k_1) logically increases with the concentration of the metal (from ≈0.04 to 0.10 min^{-1}). The Crank equation helps in roughly evaluating the effective diffusivity of In(III) in the sorbent. The D_e values vary between 0.339 × 10^{-13} m^2 min^{-1} and 1.28 × 10^{-13} m^2 min^{-1}; this variation illustrates the effect of the concentration gradient (and the fact that the controlling mechanism is a combination of different types of resistance). This value is several orders of magnitude lower than the self-diffusion coefficient of In(III) in water: Avchukir et al. [85] reported values in the range 4.2–14.4 × 10^{-9} m^2 min^{-1}, while Tehrani et al. [86] reported a value close to 2.684 × 10^{-8} m^2 min^{-1}. Kariuki et al. [87] highlighted the effect of ionic strength on the free diffusivity of indium (in the range 2.65–0.93 × 10^{-9} m^2 min^{-1}). The gap between free diffusivity and effective diffusivity in the sorbent confirms the substantial contribution of the resistance to intraparticle diffusion on the control of kinetic profiles.

Table 1
Modeling of In(III) uptake kinetics – Parameters of the models.

Modeling Model	Parameter	Unit	C_0 (mmol In L^{-1}) 0.911	4.39
Experimental	$q_{eq,exp.}$	mmol In g^{-1}	0.875	1.808
PFORE	$q_{eq,1}$	mmol In g^{-1}	0.939	1.85
	$k_1 \times 10^2$	min^{-1}	4.04	10.4
	R^2		0.945	0.982
	AIC		−81	−127
PSORE	$q_{eq,1}$	mmol In g^{-1}	1.14	2.07
	$k_2 \times 10^2$	g $mmol^{-1}$ min^{-1}	3.69	6.91
	R^2		0.905	0.938
	AIC		−74	−110
RIDE	$D_e \times 10^{13}$	m^2 min^{-1}	0.339	1.27
	R^2		0.904	0.958
	AIC		−72	−114

3.3.3. *Sorption isotherms*

The sorption isotherms are represented at four temperatures (ranging between 15 ± 1 and 50 ± 1 °C) in Fig. 4. Both the maximum sorption capacity and the initial slope of the curves decrease with increasing the temperature.

The distribution of the solute between the two phases at equilibrium is strongly controlled by the temperature. At room temperature, maximum sorption capacity reaches 1.87 mmol In g^{-1}, while at 50 °C, the sorption capacity decreases by 33%. Consistently with the preliminary results collected in the study of pH, the sorption process is exothermic. The experimental isotherm profiles have been fitted by Langmuir, Freundlich, Sips, Temkin and Dubinin-Radushkevich models (see Equations in Table S2). Table 2 summarizes the parameters of these

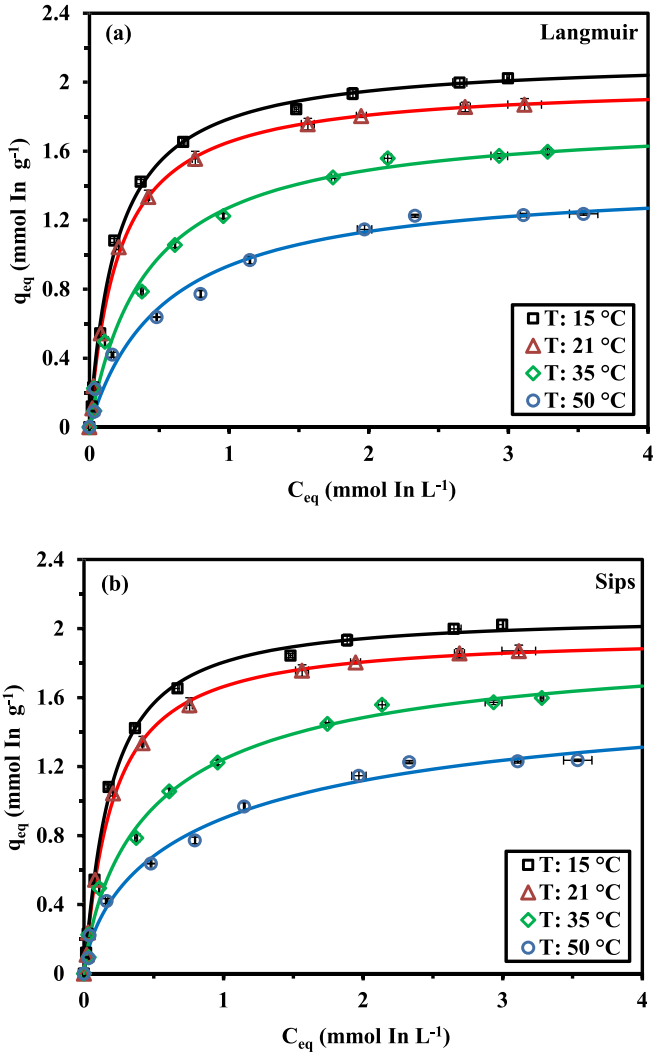

Fig. 4. In(III) sorption isotherms at pH_0 4 and T varying between 15 ± 1 °C and 50 ± 1 °C – Modeling with Langmuir (a) and Sips (b) equations (C_0: 0–4.4 mmol In L^{-1}; SD: 0.667 g L^{-1}; v: 210 rpm; time: 48 h).

Table 2
Modeling of In(III) sorption isotherms – Parameters of the models.

Modeling Model	Parameter	Unit	Temperature (°C) 15 ± 1	21 ± 1	35 ± 1	50 ± 1
Experimental	$q_{m,exp.}$	mmol In g^{-1}	2.023	1.870	1.598	1.237
Langmuir	$q_{m,L}$	mmol In g^{-1}	2.141	1.997	1.795	1.439
	b_L	L $mmol^{-1}$	5.070	4.792	2.439	1.858
	R^2		0.998	0.990	0.992	0.987
	AIC		−67	−75	−58	−58
Freundlich	k_F	$mmol^{1-1/nF}$ $L^{1/nF}$ g^{-1}	1.56	1.44	1.12	0.833
	n		3.19	3.18	2.72	2.634
	R^2		0.935	0.937	0.968	0.977
	AIC		−30	−32	−43	−53
Sips	$q_{m,S}$	mmol In g^{-1}	2.077	1.958	1.984	1.791
	b_S	$L^{1/nS}$ $mmol^{-1/nS}$	6.649	5.636	1.675	1.011
	n_S		0.899	0.936	1.21	1.39
	R^2		0.999	0.999	0.994	0.992
	AIC		−68	−75	−58	−60
Temkin	A_T	L $mmol^{-1}$	74.3	69.2	45.0	40.9
	b_T	J kg^{-1} mol^{-2}	6126	6.66	7917	10.76
	E	kJ mol^{-1}	3.03	3.56	4.96	8.70
	R^2		0.989	0.991	0.989	0.981
	AIC		−50	−54	−56	−55
D-R	q_{D-R}	mmol In g^{-1}	1.991	1.847	1.539	1.199
	$b_{DR} \times 10^8$	mol^2 kJ^2	3.14	3.10	4.39	5.14
	E_{DR}	kJ mol^{-1}	5.64	5.68	4.77	4.41
	R^2		0.997	0.997	0.970	0.957
	AIC		−65	−66	−43	−44

models (and the statistical parameters). The Langmuir and the Sips equations equally fits experimental curves, and much better than the alternative equations. The Langmuir equation is based on the monolayer sorption of the solute, without interactions between sorbed molecules and with homogeneity in the intensity and distribution of sorption sites. This equation derives from a mechanistic model based on the equalization of sorption and desorption kinetics at equilibrium. The Freundlich empiric equation is more appropriate for systems involving interactions between sorbed molecules, with heterogeneities in sorption energies. This corresponds to a power-type mathematical equation that is not consistent with the asymptotic trend of the experimental profiles. The Sips equation is actually a combination of Langmuir and Freundlich equations. The introduction of a third-adjustable parameter may increase the accuracy of the modeling at the expense of a loss in physicochemical meaning. The AIC takes into account the introduction of the third parameter. Herein, the difference in the modeling accuracy is not clearly established. The modeling of the sorption isotherms with the Langmuir and the Sips equations appears in Fig. 3. The Temkin and Dubinin-Radushkevich equations do not fit experimental profiles (though better than the Freundlich equation). The Langmuir equation overestimates the sorption capacity at saturation ($q_{eq,L}$ *vs.* $q_{eq,exp}$) by 5.8% at 15 °C and 16.3 % at 50 °C. On the opposite hand, the affinity coefficient (i.e., b_L), which is correlated with the initial slope of the curve, is substantially decreased (by a factor close to 2.7, from 4.79 L $mmol^{-1}$ to 1.86 L $mmol^{-1}$) when increasing the temperature (from 15 to 50 °C).

The decrease in In(III) sorption while increasing the temperature from 15 ± 1 to 50 ± 1 °C indicates the exothermic nature of metal sorption (Fig. 4). The thermodynamic parameters were deduced from these sorption isotherms using the van't Hoff equation and the method described by Tran et al. [88] (Figure S15):

$$\Delta G^0 = \Delta H^0 - T\Delta S^0 = -RT\ln K_{eq}^0 \quad (2a)$$

where ΔH^0 (kJ mol^{-1}) is the enthalpy change, ΔG^0 (kJ mol^{-1}) is Gibbs free energy change, and ΔS^0 (J $mol^{-1}K^{-1}$) is the entropy change.

$$\ln K_{eq}^0 = -\frac{\Delta H^0}{RT} + \frac{\Delta S^0}{R} \quad (2b)$$

With

$$K_{eq}^0 = b_L^* \times \frac{C_{Adsorbate}^0}{\gamma_{Adsorbate}} \quad (2c)$$

where b_L* is the Langmuir coefficient expressed in L mol^{-1}; $C_{Adsorbate}^0$ is the unitary standard concentration of the adsorbate (~1 mol L^{-1}), and $\gamma_{Adsorbate}$ is the activity coefficient (~1 for dilute solution).

The negative value of the enthalpy change (close to −24.2 kJ mol^{-1}) confirms the exothermic nature of indium sorption onto TcTDG (Table S4). The weakly negative value of the entropy change indicates that the entropy (randomness or disorder) of the system decreases after metal sorption. On the other side, the negative value of the Gibbs free energy (slightly decreasing with the increase of the temperature; between −20.5 kJ mol^{-1} and −20.1 kJ mol^{-1}) demonstrates that In(III) sorption onto TcTDG is spontaneous. In the case of In(III) sorption using $CoFe_2O_4$-zeolite composites, Zhao et al. [26] reported an enthalpy change close to 50.5 kJ mol^{-1} and an entropy change close to 184 J mol^{-1} K^{-1}), while the Gibbs free energy change was −4.6 kJ mol^{-1}. In the case of In(III) sorption onto chitosan-bentonite composites, Calagui et al. [25] also reported a positive value for the enthalpy change (i.e., 7.3 kJ mol^{-1}), as well as the entropy change (i.e., 29.3 J mol^{-1} K^{-1}), while the Gibbs free energy was found varying between −0.8 and −2 kJ mol^{-1}. Li et al. [89] reported that indium sorption onto extractant impregnated resins occurred as an endothermic, and spontaneous mechanism (with increased randomness while temperature increases).

The sorption properties strongly depend on the experimental conditions; the comparison with alternative sorbents is made difficult by different pH values (among other parameters). However, considering the equilibrium time together with studied pH and Langmuir parameters allows evaluating the potential of the material. The most efficient sorbent reported in Table S5 shows that nanoscale zero-valent iron has outstanding sorption capacities for In(III) (i.e., q_m ≈3.4 mmol In g^{-1}) [24]; this a little less than two times the sorption capacity reached with TcTDG. The equilibrium time and affinity coefficient are of the same orders of magnitude for the two sorbents. Apart, this specific sorbent, the sorption figures of TcDTG are globally much better than those of alternative sorbents: equilibrium contact time and maximum sorption capacities are more favorable. The less favorable parameter concerns the affinity coefficient (about 4.79 L $mmol^{-1}$, at room temperature), while other sorbents may reach much higher values (such as chitin and chitosan, [83], but with less favorable sorption capacities and kinetics). Globally, the sorption properties of TcTDG reveal promising for indium recovery from solutions containing intermediary concentrations: the sorption capacity approaches the saturation for residual concentrations as high as 2 mmol In L^{-1}.

3.3.4. *Sorption mechanisms*

Based on the results collected in the study of pH effect (and related to pH_{PZC} values) and in the FTIR characterization, it is possible identifying the different mechanisms that can be involved in In(III) sorption. Depending on the pH, and the speciation of metal ions, the binding proceeds through (a) ion-exchange/electrostatic attraction (for example: anionic species interact with protonated amine groups or the ion-exchange of protons with cation species) and (b) chelation onto amine groups, or thiocarbonyl groups. The different mechanisms are summarized in Scheme 2. Based on the coordination number (CN: 6) different reactive groups may be simultaneously involved (combined with the effects of indium hydration, hydrolysis, or complexation). The bifunctionnalization brings a high density of reactive groups (compared with mono-aminophosphonation), which, in turn, may cause steric hindrance and/or favorable steric arrangement of functional groups (accommodating the indium species). Apparently, the high efficiency of

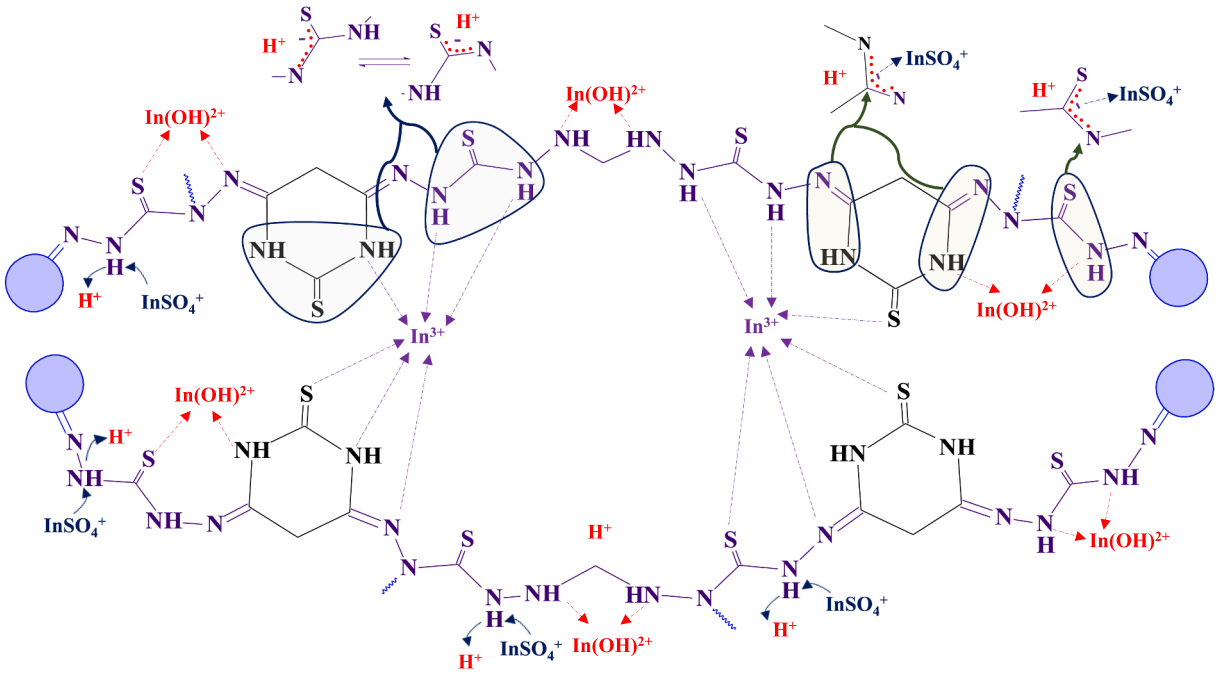

Scheme 2. Tentative mechanisms involved In(III) sorption onto TcTDG.

Tc-TDG sorbents for In(III) binding tends to indicate that the steric arrangement effect is more effective than the steric hindrance impact.

3.3.5. *Sorption selectivity*

Indium being generally obtained as a by-product of the extraction of other metals [1,8,90,91], one of the key-factor concerns the selectivity of the sorbent for In(III) in complex multi-component solutions. To address this question, the sorption of In(III) using TcTDG was processed from multi-component equimolar solutions (i.e., at 1 mmol L^{-1}) at different pH values. Fig. 5 compares the distribution ratio and the selectivity coefficient $SC_{In/metal}$. The distribution ratios (Fig. 5a) remain very low for Mg(II), Ca(II), Zn(II), Al(III) and Fe(III) (systematically below 0.23 L g^{-1}); the D value systematically increases with pH augmentation (in the pH range: 2.28–5.14). The same pH effect is observed for Ga(III), and Ce(III). It is noteworthy that the relative ranking of D values (L g^{-1}) globally follows the order at pH 5.24–5.87:

Zn(II)[0.114]≈Ca(II)≈Mg(II)≈Al(III) < Fe(III) < In(III)[0.405]≈Ga(III) < Ce(III)[0.534].

The sorbent as a clear preference for trivalent metal ions. The figure also shows that In(III) follows a different trend than other elements with an optimum pH found close to pH_{eq} 4.19.

At this optimum pH value, the ranking of affinity of the sorbent for target metals follows:

Mg(II)[0.028] < Al(III) < Zn(II) < Ca(II) < Fe(III)[0.166] < Ga(III)≈Ce(III)[0.324]≪In(III)[0.983].

At pH ≈4.2, the differences are more marked between In(III) and the other trivalent metal ions (and more favorable to indium). This is confirmed by the corresponding plots of $SC_{In/metal}$ values (Fig. 5b). The highest selectivity is obtained at pH 4.19, with preference order:

In(III)[1]≫Ce(III)≈Ga(III)[3.06]≫Fe(III)[5.94]≫Ca(II)[10.5] > Zn(II) > Al(III)[16]≫Mg(II)[35.5].

The variation on selectivity with pH may be correlated with the effect of protonation/deprotonation of reactive groups (meaning also the change in the sorption mechanism) and/or the speciation of specific metal ions. In strongly acidic solutions, the protonation of amine groups mainly engages ion-exchange mechanisms (exchange of protons with metal cations, or the binding of anionic species on protonated reactive groups), while at higher pH (neutral and above) chelation is enhanced: the metals with higher affinity for chelation onto N-ligands are expected to be readily bound with decrease in their relative selectivity coefficient. Tokuyama et al. [92] synthesized an impregnated sorbent (actually an emulsion gel, associating an acrylate derivative and an organophosphorus extractant) for the sorption of rare metal ions. They showed that the In(III)/Zn(II) separation is controlled by the pH. In acidic solutions, zinc species are poorly bound in acidic solutions, while In(III) uptake (though decreased) maintains non-negligible sorption. As the pH increases, the simultaneous (improved) sorption of both In(III) and Zn(II) leads to a decrease in the selective separation.

The selectivity of the sorbent for In(III) strongly depends on the pH, which affects both the ranking of the different metal ions as well as the order of magnitude, as shown on the classifications (number into brackets gives the relevant $SC_{In/metal}$ values).

pH_{eq} 2.28: Mg(21)≫Ca, Al(7.3) > Ga(7.0)≫Fe, Zn(3.8) > Ce(3.2).

pH_{eq} 3.22: Mg(32)≫Al(11) > Zn(9.1) > Ca(6.6) > Fe(5.5) > Ce, Ga (3.4).

pH_{eq} 4.19: Mg(35)≫Al(16) > Zn(14)≫Ca(10)≫Fe(5.9) > Ga, Ce (3.0).

pH_{eq} 5.14: Mg(6.0) > Zn(5.6) > Ca(5.0) > Al(4.2)≫Fe(2.7)≫Ga (1.3) > Ce(1.0).

pH_{eq} 5.87: Zn(3.5) > Ca, Mg(3.3) > Al(3.1) > Fe(1.8) > Ga(0.97) > Ce(0.76).

At pH above 5, the selectivity of the sorbent for In(III) is strongly depreciated. At optimum acidic pH (i.e., pH_{eq} 4.19, the most representative for high indium recovery), the key pattern for selectivity is especially marked against Mg, Al, Zn, Ca, and Fe, while the sorbent exhibits lower selectivity against Ga and Ce (which have closer chemistry to indium). However, it is noteworthy that despite this lower selectivity for Ce(III) and Ga(III), the sorbent maintains a higher preferential affinity for indium at this pH than at higher pH values. Hence, at pH 5.87 the sorbent even has a lightly higher selectivity for Ce(III) than for In(III).

The sorbent has a marked selectivity for trivalent metal ions against other tested metal ions (with the remarkable exception of Al(III)). Figure S16 shows the impact of the position of metal ions in the Covalent Index ($X_m^2 \times r$) *vs.* Ionic Index (z^2 / r) space ([93]) on the distribution ratio: the bubble size is proportional to D_{metal} value. X_m is the Pauling

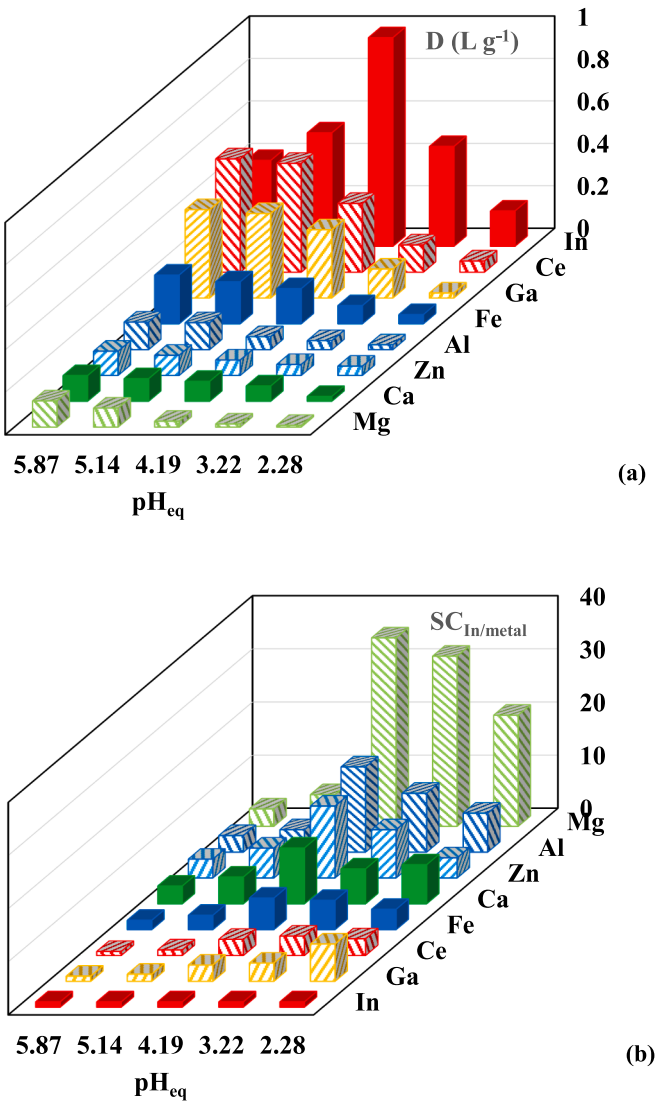

Fig. 5. Sorption from multi-component equimolar solutions: (a) distribution ratio D and (b) $SC_{In/metal}$ (C_0: ≈1 mmol L^{-1}; SD: 1 g L^{-1}; time: 24 h; T: 21 ± 1 °C; $SC_{In/In}$ = 1 as reference).

electronegativity, r the hydrated ion radius, and z the ionic charge of the target element. In(III), Fe(III), Ga(III), and Zn(II) are localized in the intermediate region (borderline elements), while Ca(II), Mg(II), Ce(III), and Al(III) are members of the Class A elements [93]. Therefore, it is not possible directly correlating the affinity of the sorbent for these metals (based on distribution ratio or selectivity coefficient) to their classification according the HSAB theory [94]. Based on the HSAB principles, hard metals have higher affinity for hard bases. N-bearing ligands, as intermediary/soft bases, are stronger than S-bearing ligands (which are strictly ranked among soft bases). The weaker electronegativity of sulfur (from thiocarbonyl) compared with nitrogen (in amine or pyrimidine moieties) allows the binding of soft metals through the available electron pairs; this activity may be favored by tautomerization effects.

In the case of phosphorylated sawdust, despite the preference of the sorbent for In(III) over Zn(II), the recovery of target metal is not sufficient to achieve its selective separation [95]. The ion-imprinting of silica functionalized with vinylphosphonic and allyl mercaptan allowed designing a selective sorbent for In(III) [96]: the presence of competitor ions, even in large excess hardly affected the sorption of target metal (both in batch and fixed-bed reactors). Li et al. [96] explained the selectivity by the appropriate matching of the imprinted cavity with the size and geometry of In(III). Li et al. [27] described the functionalization of aminated silica gel/graphene oxide by reaction with vinylphosphinic acid, and the synthesis of an ion-imprinting derivative for the selective recovery of indium(III) from a series of binary solutions. The imprinting process strongly increases the distribution ratio for In(III) with limited effect on the sorption of other metals: the selectivity is strongly improved by ion-imprinting (by a factor 8.5 to 10.8). The lowest selectivity was obtained against Fe(III) (i.e., 8.5, while for divalent cations the selectivity coefficient varies between 16.7 and 35.3). The higher affinity for In(III) and other hard acids was associated with the hard-base character of phosphonic moieties (opposed to borderline metal ions). However, they also pointed out the importance of coordination geometry and ionic radius. In the case of solvent impregnated resins (EHEHPA-extractant/HZ818-resin), Yuan et al. [18] played with the pH effect for separating In(III) (optimized at pH 1.5) from Zn(II) (which requires higher pH value for sorption, above pH 3.5). In the selectivity study for In(III) sorption in binary solutions using hydroxyl/amine resins, Li et al. [27] claimed the selectivity to be driven by the charge hold by indium: trivalent ion showing higher chelation with the hydroxyl and amine groups than divalent or monovalent metal ions.

3.3.6. *Metal desorption and sorbent recycling*

The potential of a newly designed sorbent cannot be evaluated without considering the reuse of the sorbent. Different eluents can be used for desorbing indium from loaded sorbents. Marinho et al. [97] successfully used EDTA (0.1 M) solution for eluting In(III) from strong basic anionic resins. However, acidic solutions are more frequently used for achieving the desorption of In(III) [29,33,96]. Alguacil et al. [29] used 1 M H_2SO_4 solution for desorbing indium from carbon nanotube (efficiency close to 75%). In the case of Lewatit TP207 (imminodiacetate resin), Lee et al. [33] used HCl and H_2SO_4 solutions at pH 0.8 for complete release of In(III). Li et al. [27] preferred using 2 M H_2SO_4 solution for total elution of In(III) from composite ion-imprinted polymer. Herein, 0.3 M HCl solution was selected and tested for evaluating the desorption kinetics (Figure S17). Desorption tests were performed on the samples collected at the end of the study of uptake kinetics (i.e., obtained with two different metal concentrations). The effective loading of the sorbents does not significantly affect the kinetic profile of In(III) desorption: the equilibrium is systematically reached in 20–30 min of contact.

Based on these results, 0.3 M HCl solution was used for testing the reuse of the sorbent for five cycles (with a rinsing step being systematically operated between each step using demineralized water). Table 3 compares the sorption and desorption efficiencies. Indium desorption is complete along the successive re-uses. On the other hand, the sorption capacity progressively decreases (from 64.2% to 61.9%). At the fifth cycle, the loss in sorption efficiency remains below 3.6%. This result confirms the high stability of the sorbent at recycling. This is consistent

Table 3
Sorption and desorption performances (efficiencies) at sorbent recycling.

In(III) concentration for loading	C_0: 0.911 mmol In L^{-1}		C_0: 4.39 mmol In L^{-1}	
Cycle	SE (%)	DE (%)	SE (%)	DE (%)
1	64.2 ± 1.0	100.6 ± 0.4	28.0 ± 1.3	100.1 ± 0.9
2	63.4 ± 1.2	100.1 ± 0.4	27.8 ± 1.3	100.0 ± 0.2
3	62.8 ± 0.6	99.8 ± 0.0	27.6 ± 1.3	99.9 ± 0.4
4	64.2 ± 1.0	100.0 ± 0.4	27.2 ± 1.3	100.2 ± 0.4
5	64.2 ± 1.0	100.5 ± 0.2	27.0 ± 1.2	100.0 ± 0.2
Loss in sorption at 5th cycle	3.6%	negligible		negligible

Experimental conditions: In(III)-loaded samples collected from uptake kinetics; desorption: 0.3 M HCl eluent; SD = 2 g L^{-1}; time = 2 h; T = 21 ± 1 °C).

with the FTIR analysis operated on the sorbent after being used along five sorption/desorption cycles (see Section 3.2.4. and Fig. 1). Although it would still be necessary to carry out a greater number of cycles to asses more precisely the economic potential of this new material; these first results demonstrate its promising performances.

3.4. Application to mining effluent

3.4.1. Ore leachate

Another important step in the evaluation of the potential of TcTDG for In(III) recovery concerns the verification of sorption performance in the treatment of real complex effluents. This complementary test was performed on leachate of an ore collected from Abu Dabbab mining area (Centre Eastern Desert, Egypt). This mineral resource contains a wide range of heavy and rare metals; more information on the location of the mining deposit (Figure S18) and the composition of the ore (Table S6 and Figure S19) is available in Section D in Supplementary Information. The acid leaching was operated in batch under selected experimental conditions [98]: grinded ore sample (less than 60 Mesh) was leached with 8 M HCl solution with a solid/liquid ratio 1:5 (30 g per 150 mL; in presence of sodium perchlorate as oxidizing agent, with 1:15 ratio between the ore and the oxidant) at 75 °C for 8 h (under agitation; V = 250 rpm). The leachate was completed with the washing effluent (water) of ore residue, to reach a final volume of 300 mL. The composition of the leachate (trace valorizable metal ions) is reported in Table S7, together with their leaching efficiency. Rare metals (gallium and indium) are recovered with yield as high as 95% (with concentrations as high as 247 and 171 mg L^{-1}). Iron is also leached with high efficiency (about 77%), leading to huge concentration (i.e., ≈7900 mg L^{-1}). The investigation of indium recovery from the leachates is carried out at different pH values (from 1 to 5). Due to the large concentration of iron, controlling the pH to weak acidic conditions leads to iron precipitation and co-precipitation of other metal ions present in the leachate. Figure S20 reports the precipitation yields for selected metal ions at different pH_{eq} values. Table S8 highlights metal precipitation at pH 5: iron is almost completely precipitated, while the other base metals (or elements) are precipitated with yields of 3.7% (sodium) to 41% (strontium); precipitation yields up to 39% for gallium and 56% for indium. This precipitation mechanism has been taken into account to calculate the effective sorption capacity of individual metals (i.e., corrected from the fraction of metal precipitated).

3.4.2. Sorption process.

Fig. 6a shows the log_{10} plot of distribution ratio *vs.* pH_{eq} for selected metals. As expected, the distribution ratios increase with the pH. The highest values are obtained for In(III), Sr(II), and Ga(III). Indium sorption capacity is close to 0.113 ± 0.008 mmol In g^{-1} in a broad pH range (i.e., 1.83–4.96), the correction of initial concentration due to metal precipitation levels the effect of pH on effective sorption capacity. At pH_{eq} 3.98, the sorption capacity is 0.122 mmol In g^{-1} in equilibrium with a residual concentration of 0.245 mmol In L^{-1}; this is almost 9 times lower than the level reached for In(III) sorption from mono-component synthetic solution (Fig. 4). The complexity of the solution and the presence of a huge excess of other metals drastically reduces indium recovery. In the case of Ga(III) sorption capacity reaches up to 0.296 ± 0.002 mmol Ga g^{-1} at pH 3.98–4.96 (in equilibrium with residuals concentrations in the range 0.58–0.74 mmol Ga L^{-1}).

The selectivity coefficients $SC_{In/metal}$ are plotted *vs* pH_{eq} in Fig. 6b. Except in the case of Fe(III), the highest SC values are obtained at pH_{eq} 4.96. For Fe(III), $SC_{In/metal}$ reaches a maximum at pH_{eq} 1.83 (at this pH, iron weakly precipitates and the huge excess of iron leads to poor distribution ratio; i.e., log_{10} D_{Fe} = -2.59). At pH 4.96, the selectivity of TcTDG for In(III) decreases according to the series:

Na(I)[47]≫Mn(II)[28.7]≫Si(IV)[17.3] > Ba(II)[15] > Fe(III)[13.6]≫Ga(III)[6.4] > Sr(II)[4.7].

The distribution of selected metals between the three compartments

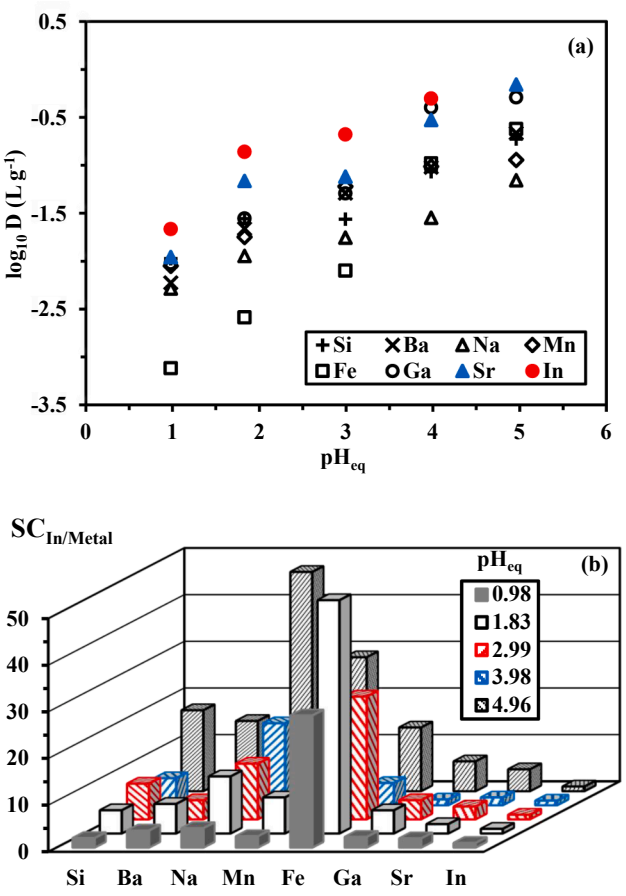

Fig. 6. Application of TcTDG to the treatment of ore leachate: (a) distribution ratio D and (b) $SC_{In/metal}$ (SD: 5 g L^{-1}; time: 10 h; T: 21 ± 1 °C).

(precipitate, sorbent, and effluent) can be summarized at pH_0: 3, 4, and 5, in Figure S21. These figures show the difficulty to separate indium (and more generally the rare metals) from these complex solutions. The main conclusions may be summarized by the following patterns:

(a) At pH_0 4 and 5, iron is removed as a precipitate that contains substantial fractions of Si(IV), Ba(II), Mn(II), Ga(III), Sr(II), and In(III).

(b) At pH_0 5, the loss of indium in the aqueous residue is minimized (less than 2.6%), but a significant fraction of the metal is present in the iron-based precipitate (i.e., ≈56%); the accumulation of indium reaches 41.3% (this is more or less the same percentage as at pH_0 4; i.e., 43%).

(c) The precipitates are multi-metallic and the sorbent contains quantifiable amounts of each of selected metals with difficulty to separate valuable metals from other co-existing elements.

The broad reactivity of TcTDG is confirmed by the semi-quantitative EDX analysis of the sorbent after being exposed to the leachate (Figure S22): a wide spectrum of metal and elements are identified at the surface of particles. The atomic concentration for sorbent compartment (C and N elements) are roughly conserved; the increase in S fraction at pH 5 (compared with pH 3) suggests that some metal ions are bound under their sulfate form. At pH_0 3, the atomic concentrations for the different heavy and rare metals are roughly of the same order of magnitude (between 1.16% for Mg(II) and 3.82% for Al(III)) even for the metals in excess in the solution (such as Fe(III) at 127-fold, and Mn(II) or Ga(III), with 2- and 3-fold concentrations, respectively). Despite the relatively lower In(III) concentration in the solution, its enrichment in the sorbent is improved compared with other elements. This is even more important in the case of pH_0 5.

4. Conclusion

The readily synthesis of this new material by the formaldehyde-mediated condensation of thiobarbituric acid and thiocarbazide (two commercial products that were synthesized here from their precursors) allows producing an efficient sorbent for In(III) recovery from weakly acidic solutions. The high density of N-bearing groups and the presence (in lower amounts) of S-bearing groups explain the binding of the trivalent cation. Despite the poor textural properties of the sorbent, its use as micro-particles makes the kinetics relatively fast. The sorbent reveals one of the most efficient sorbent for indium recovery, when compared with recent literature (and considering both the pH, the equilibrium time, and Langmuir criteria). Fast and complete desorption is also observed when using acidic solutions (0.3 M HCl) with good stability at recycling (full desorption and decrease in sorption at the fifth cycle lower than 3.6%). In multi-component solutions (at equimolar concentration), the sorbent shows preference for In(III) at pH 4 against trivalent cations with even more marked selectivity against mono- and di-valent base elements. This trend is also respected for complex ore leachate; although the complexity of the effluent (huge concentrations of iron and some other base metals) significantly reduces the sorption capacities for the recovery of valuable metal ions (such as indium and gallium). These promising results justify complementary work to design other conditioning of these materials with enhanced textural properties to prepare larger particles (for facilitated application at large scale), having higher specific surface area, and improved porosity (use of porogen, drying method, etc.). The proper evaluation of the processing costs would also require extending the number of recycling steps applicable for the treatment of real effluents.

CRediT authorship contribution statement

Mohammed F. Hamza: Conceptualization, Methodology, Supervision, Writing – review & editing. **Abd Allh M. Abd El-Hamid:** Formal analysis, Investigation, Resources. **Eric Guibal:** Conceptualization, Software, Formal analysis, Data curation, Writing – review & editing. **Adel A.-H. Abdel-Rahman:** Supervision, Investigation. **Rania El Araby:** Methodology, Formal analysis.

Declaration of Competing Interest

The authors declare that they have no known competing financial interests or personal relationships that could have appeared to influence the work reported in this paper.

Data availability

Data will be made available on request.

Appendix A. Supplementary data

Supplementary data to this article can be found online at https://doi.org/10.1016/j.seppur.2023.123514.

References

[1] A.M. Alfantazi, R.r., Moskalyk, Processing of indium: a review, Miner. Eng. 16 (2003) 687–694, https://doi.org/10.1016/s0892-6875(03)00168-7.

[2] S. Dhiman, B. Gupta, Cyphos IL 104 assisted extraction of indium and recycling of indium, tin and zinc from discarded LCD screen, Sep. Purif. Technol. 237 (2020), 116407, https://doi.org/10.1016/j.seppur.2019.116407.

[3] J. Qin, S. Ning, J. Xu, F. Guo, Z. Li, Y. Wei, G. Dodbiba, T. Fujita, Study on the adsorption behavior of tin from waste liquid crystal display using a novel macroporous silica-based adsorbent in one-step separation, Sep. Purif. Technol., 292 (2022) 121006 (https://doi.org/10.1016/j.seppur.2022.121006).

[4] S. Ishihara, H. Matsueda, Chemical characteristics of the indium-polymetallic ores from the Toyoha mine, Hokkaido, Japan, Bull. Geol. Surv. Jpn. 62 (2011) 131–142, https://doi.org/10.9795/bullgsj.62.131.

[5] D. Pradhan, S. Panda, L.B. Sukla, Recent advances in indium metallurgy: A review, Miner. Process. Extr. Metall. Rev. 39 (2018) 167–180, https://doi.org/10.1080/08827508.2017.1399887.

[6] E. Commission, Study on the review of the list of critical raw materials, Publications Office, 2017 final report,.

[7] M. Assefi, S. Maroufi, R.K. Nekouei, V. Sahajwalla, Selective recovery of indium from scrap LCD panels using macroporous resins, J. Cleaner Prod. 180 (2018) 814–822, https://doi.org/10.1016/j.jclepro.2018.01.165.

[8] A.J. Whitworth, J. Vaughan, G. Southam, A. van der Ent, P.N. Nkrumah, X. Ma, A. Parbhakar-Fox, Review on metal extraction technologies suitable for critical metal recovery from mining and processing wastes, Miner. Eng. 182 (2022), 107537, https://doi.org/10.1016/j.mineng.2022.107537.

[9] L. Zhang, Z. Xu, A critical review of material flow, recycling technologies, challenges and future strategy for scattered metals from minerals to wastes, J. Cleaner Prod. 202 (2018) 1001–1025, https://doi.org/10.1016/j.jclepro.2018.08.073.

[10] Y.-F. Huang, S.-Y. Wang, S.-L. Lo, Indium recovery from spent liquid crystal displays by using hydrometallurgical methods and microwave pyrolysis, Chemosphere 280 (2021), 130905, https://doi.org/10.1016/j.chemosphere.2021.130905.

[11] J.E. De-la-Cruz-Moreno, A.E. Ceniceros-Gomez, O. Morton-Bermea, E. Hernandez-Alvarez, Recovery of indium from jarosite residues of zinc refinery by a hydrometallurgical process, Hydrometallurgy 203 (2021), 105697, https://doi.org/10.1016/j.hydromet.2021.105697.

[12] M. Drzazga, A. Palmowski, G. Benke, M. Ciszewski, K. Leszczynska-Sejda, Recovery of germanium and indium from leaching solution of germanium dross using solvent extraction with TOA, TBP and D2EHPA, Hydrometallurgy 202 (2021), 105605, https://doi.org/10.1016/j.hydromet.2021.105605.

[13] Z. Deng, X. Li, C. Wei, G. Fan, M. Li, C. Li, Recovery of indium from hard zinc slag by pressure leaching and solvent extraction, Jom 73 (2021) 721–728, https://doi.org/10.1007/s11837-020-04519-4.

[14] E.B. Pereira, A.L. Suliman, E.H. Tanabe, D.A. Bertuol, Recovery of indium from liquid crystal displays of discarded mobile phones using solvent extraction, Miner. Eng. 119 (2018) 67–72, https://doi.org/10.1016/j.mineng.2018.01.022.

[15] S. Nusen, T. Chairuangsri, Z. Zhu, C.Y. Cheng, Recovery of indium and gallium from synthetic leach solution of zinc refinery residues using synergistic solvent extraction with LIX 63 and Versatic 10 acid, Hydrometallurgy 160 (2016) 137–146, https://doi.org/10.1016/j.hydromet.2016.01.007.

[16] C. Deferm, B. Onghena, T. Vander Hoogerstraete, D. Banerjee, J. Luyten, H. Oosterhof, J. Fransaer, K. Binnemans, Speciation of indium(III) chloro complexes in the solvent extraction process from chloride aqueous solutions to ionic liquids, Dalton Trans. 46 (2017) 4412–4421, https://doi.org/10.1039/c7dt00618g.

[17] F.J. Alguacil, I. Garcia-Diaz, E. Escudero, Extraction of indium(III) from sulphuric acid medium by the ionic liquid (PJMTH(+)HSO(4) (-)), Sep. Purif. Technol. 211 (2019) 764–767, https://doi.org/10.1016/j.seppur.2018.10.051.

[18] Y. Yuan, J. Liu, B. Zhou, S. Yao, H. Li, W. Xu, Synthesis of coated solvent impregnated resin for the adsorption of indium (III), Hydrometallurgy 101 (2010) 148–155, https://doi.org/10.1016/j.hydromet.2009.12.010.

[19] J.S. Liu, Z.G. He, J. Cai, C.G. Cai, B.X. Zhou, W.M. Cai, Separation of indium (III), gallium (III), and zinc (II) with Levextrel resin containing di(2-ethylhexyl) phosphoric acid (CL-P204): Part I, Selection of separation conditions, Rare Met. 22 (2003) 235–240.

[20] S. Van Roosendael, M. Regadio, J. Roosen, K. Binnemans, Selective recovery of indium from iron-rich solutions using an Aliquat 336 iodide supported ionic liquid phase (SILP), Sep. Purif. Technol. 212 (2019) 843–853, https://doi.org/10.1016/j.seppur.2018.11.092.

[21] F.-C. Yen, T.-C. Chang, S. Laohaprapanon, Y.-L. Chen, S.-J. You, Recovery of indium from LCD waste by solvent extraction and the supported liquid membrane with strip dispersion using D2EHPA as the extractant, Solvent Extr. Res. Dev. - Jpn. 23 (2016) 63–73.

[22] T.H. Nguyen, M.S. Lee, A review on separation of gallium and indium from leach liquors by solvent extraction and ion exchange, Miner. Process. Extr. Metall. Rev. 40 (2019) 278–291, https://doi.org/10.1080/08827508.2018.1538987.

[23] K.L. Timofeev, G.I. Maltsev, A.V. Sviridov, Indium extraction from solutions with modified aluminosilicates, Izvestiya Vysshikh Uchebnykh Zavedenii Khimiya I Khimicheskaya Tekhnologiya 59 (2016) 35–41.

[24] W. Chen, Y. Su, Z. Wen, Y. Zhang, X. Zhou, C. Dai, Recovery of indium ions by nanoscale zero-valent iron, J. Nanopart. Res. 19 (2017), https://doi.org/10.1007/s11051-016-3692-7.

[25] M.J.C. Calagui, D.B. Senoro, C.-C. Kan, J.W.L. Salvacion, C.M. Futalan, M.-W. Wan, Adsorption of indium(III) ions from aqueous solution using chitosan-coated bentonite beads, J. Hazard. Mater. 277 (2014) 120–126, https://doi.org/10.1016/j.jhazmat.2014.04.043.

[26] F. Zhao, Y. Zou, X. Lv, H. Liang, Q. Jia, W. Ning, Synthesis of $CoFe_2O_4$-zeolite materials and application to the adsorption of gallium and indium, J. Chem. Eng. Data 60 (2015) 1338–1344, https://doi.org/10.1021/je501039u.

[27] M. Li, S. Tang, R. Liu, X. Meng, J. Feng, L. Zhou, Y. Chen, Experimental and DFT studies on highly selective separation of indium ions using silica gel/graphene oxide based ion-imprinted composites as a sorbent, Chem. Eng. Res. Des. 168 (2021) 135–145, https://doi.org/10.1016/j.cherd.2021.01.033.

[28] W. Zeng, L. Xu, Q. Wang, C. Chen, M. Fu, Adsorption of indium(III) ions from an acidic solution by using UiO-66, Metals 12 (2022) 579.

[29] F.J. Alguacil, F.A. Lopez, O. Rodriguez, S. Martinez-Ramirez, I. Garcia-Diaz, Sorption of indium (III) onto carbon nanotubes, Ecotoxicol. Environ. Saf. 130 (2016) 81–86, https://doi.org/10.1016/j.ecoenv.2016.04.008.

[30] L.-H. Wang, Z.-H. Qiu, L.-S. Chi, Graphene oxide/Fe_3O_4 magnetic nanocomposites for efficient recovery of indium, Chin. J. Struct. Chem. 40 (2021) 1423–1432, https://doi.org/10.14102/j.cnki.0254-5861.2011-3161.

[31] H. Zhang, X. Chen, C. Xiong, C. Yao, J. Li, X. Zheng, J. Jiang, Adsorption of Indium (III) from aqueous solutions using SQD-85 resin, Indian, J Chem. Technol. 22 (2015) 113–119.

[32] M.C.B. Fortes, A.H. Martins, J.S. Benedetto, Selective separation of indium by iminodiacetic acid chelating resin, Braz. J. Chem. Eng., 24 (2007) 287-292 (https://doi.org/10.1590/s0104-66322007000200013).

[33] S.-K. Lee, U.H. Lee, Adsorption and desorption property of iminodiacetate resin (Lewatit (R) TP207) for indium recovery, J. Ind. Eng. Chem., 40 (2016) 23-25 (https://doi.org/10.1016/j.jiec.2016.05.016).

[34] Y. Akama, S. Suzuki, Y. Monobe, Study on the adsorption and selective separation of indium from zinc with chelating cellulose, Cellul. Chem. Technol. 50 (2016) 147–152.

[35] M.C.B. Fortes, A.H. Martins, J.S. Benedetto, Indium adsorption onto ion exchange polymeric resins, Miner. Eng., 16 (2003) 659-663 (https://doi.org/10.1016/s0892-6875(03)00130-4).

[36] C. Fortin-Lecomte, L.-H. Tran, G. Rioux, L. Coudert, J.-F. Blais, Recovery of indium from acidic leach solutions of spent LCD panels using ion exchange, Hydrometallurgy, 210 (2022) 105845 (https://doi.org/10.1016/j.hydromet.2022.105845).

[37] G. Li, B. Zhang, Z. Ma, Z. Wang, Facile synthesis of hydroxyl- and amine-riched porous polymer for indium recovery in water, Microporous Mesoporous Mater., 323 (2021) 111162 (https://doi.org/10.1016/j.micromeso.2021.111162).

[38] N.I. Gorshkov, A.Y. Murko, I.I. Gavrilova, M.A. Bezrukova, A.I. Kipper, V.D. Krasikov, E.F. Panarin, Synthesis of water-soluble copolymers of N-vinylpyrrolidone with N-vinyldithiocarbamate as multidentate polymeric chelation systems and their complexes with indium and gallium, Molecules, 25 (2020) 4681 (https://doi.org/10.3390/molecules25204681).

[39] Z. Li, G.L. Dotto, A. Bajahzar, L. Sellaoui, H. Belmabrouk, A. Ben Lamine, A. Bonilla-Petriciolet, Adsorption of indium (III) from aqueous solution on raw, ultrasound- and supercritical-modified chitin: Experimental and theoretical analysis, Chem. Eng. J., 373 (2019) 1247-1253 (https://doi.org/10.1016/j.cej.2019.05.134).

[40] W. Guo, J. Zhang, F. Yang, F. Tan, Z. Zhao, Highly efficient and selective recovery of gallium achieved on an amide-functionalized cellulose, Sep. Purif. Technol., 237 (2020) 116355 (https://doi.org/10.1016/j.seppur.2019.116355).

[41] J. Du, M. Zhang, Z. Dong, X. Yang, L. Zhao, Facile fabrication of tannic acid functionalized microcrystalline cellulose for selective recovery of Ga(III) and In(III) from potential leaching solution, Sep. Purif. Technol., 286 (2022) 120442 (https://doi.org/10.1016/j.seppur.2022.120442).

[42] J. Roosen, S. Mullens, K. Binnemans, Multifunctional alginate-sulfonate-silica sphere-shaped adsorbent particles for the recovery of indium(III) from secondary resources, Ind. Eng. Chem. Res., 56 (2017) 8677-8688 (https://doi.org/10.1021/acs.iecr.7b01101).

[43] X.H. Pan, J.H. Zu, J.J. Diao, Y. Xue, S.Y. Liu, Rapid and selective recovery of Ag(I) from simulative electroplating effluents by sulfydryl-rich covalent organic framework (COF-SH) with high adsorption capacity, Colloids Surf., A, 648 (2022) 129156 (https://doi.org/10.1016/j.colsurfa.2022.129156).

[44] C.-A. Ghiorghita, K.B.L. Borchert, A.-L. Vasiliu, M.-M. Zaharia, D. Schwarz, M. Mihai, Porous thiourea-grafted-chitosan hydrogels: Synthesis and sorption of toxic metal ions from contaminated waters, Colloids Surf., A, 607 (2020) 125504 (https://doi.org/https://doi.org/10.1016/j.colsurfa.2020.125504).

[45] L. Zhang, Y. Zhao, C. Mu, X. Zhang, Selective adsorption for Ag (I) from wastewater by carbon-magnetic fly ash beads modified with polydopamine and thiourea, Sustainable Chem. Pharm., 17 (2020) 100287 (https://doi.org/https://doi.org/10.1016/j.scp.2020.100287).

[46] M.H. Amini, M.H. Beyki, Water detoxification in terms of lead (II) and *Bacillus subtilis* bacteria using poly thiourea resin fabricated on magnetic multiwall carbon nanotubes substrate, Polym. Bull., 10.1007/s00289-022-04265-4 (2022) (https://doi.org/10.1007/s00289-022-04265-4).

[47] M.F. Hamza, Y. Wei, M.S. Khalafalla, N.S. Abed, A. Fouda, K.Z. Elwakeel, E. Guibal, N.A. Hamad, U(VI) and Th(IV) recovery using silica beads functionalized with urea- or thiourea-based polymers - Application to ore leachate, Sci. Total Environ., 821 (2022) 153184 (https://doi.org/10.1016/j.scitotenv.2022.153184).

[48] M. Hussain, N. Maile, K. Tahir, A.A. Ghani, B. Kim, J. Jang, D.S. Lee, Flexible thiourea-based covalent organic frameworks for ultrahigh mercury removal from aqueous solutions, Chem. Eng. J., 446 (2022) 137410 (https://doi.org/https://doi.org/10.1016/j.cej.2022.137410).

[49] L.-Y. Yuan, Z.-Q. Bai, R. Zhao, Y.-L. Liu, Z.-J. Li, S.-Q. Chu, L.-R. Zheng, J. Zhang, Y.-L. Zhao, Z.-F. Chai, W.-Q. Shi, Introduction of bifunctional groups into mesoporous silica for enhancing uptake of thorium(IV) from aqueous solution, ACS Appl. Mater. Interfaces, 6 (2014) 4786-4796 (https://doi.org/10.1021/am405584h).

[50] S.D. Alexandratos, X.P. Zhu, M. Florent, R. Sellin, Polymer-supported bifunctional amidoximes for the sorption of uranium from seawater, Ind. Eng. Chem. Res., 55 (2016) 4208-4216 (https://doi.org/10.1021/acs.iecr.5b03742).

[51] S.A. Younis, M.M. Ghobashy, G. Bassioni, A.K. Gupta, Tailored functionalized polymer nanoparticles using gamma radiation for selected adsorption of barium and strontium in oilfield wastewater, Arabian J. Chem., 13 (2020) 3762-3774 (https://doi.org/10.1016/j.arabjc.2018.12.010).

[52] Y. Wei, M. Rakhatkyzy, K.A.M. Salih, K. Wang, M.F. Hamza, E. Guibal, Controlled bi-functionalization of silica microbeads through grafting of amidoxime/methacrylic acid for Sr(II) enhanced sorption, Chem. Eng. J., 402 (2020) 125220 (https://doi.org/10.1016/j.cej.2020.125220).

[53] O. Dudarko, N. Kobylinska, B. Mishra, V.G. Kessler, B.P. Tripathi, G.A. Seisenbaeva, Facile strategies for synthesis of functionalized mesoporous silicas for the removal of rare-earth elements and heavy metals from aqueous systems, Microporous Mesoporous Mater., 315 (2021) 110919 (https://doi.org/10.1016/j.micromeso.2021.110919).

[54] Z. Ahmad, Y. Li, S. Ali, J. Yang, F. Jan, Y. Fan, X. Gou, Q. Sun, J. Chen, Benignly-fabricated supramolecular poly(amidoxime)-alginate-poly(acrylic acid) beads synergistically enhance uranyl capture from seawater, Chem. Eng. J., 441 (2022) 136076 (https://doi.org/10.1016/j.cej.2022.136076).

[55] L. Jing, S. Yang, X. Li, Y. Jiang, J. Lou, Z. Liu, Q. Ding, W. Han, Effective adsorption and sensitive detection of Cr^{6+} by degradable collagen-based porous fluorescent aerogel, Ind. Crops Prod., 182 (2022) 114882 (https://doi.org/10.1016/j.indcrop.2022.114882).

[56] M. Imamoglu, D. Perez-Quintanilla, I. Sierra, Bifunctional periodic mesoporous organosilicas with sulfide bridges as effective sorbents for Hg(II) extraction from environmental and drinking waters, Microporous Mesoporous Mater., 229 (2016) 90-97 (https://doi.org/10.1016/j.micromeso.2016.04.023).

[57] Z. Ahmad, Y. Li, J. Yang, N. Geng, Y. Fan, X. Gou, Q. Sun, J. Chen, A membrane-supported bifunctional poly(amidoxime-ethyleneimine) network for enhanced uranium extraction from seawater and wastewater, J. Hazard. Mater., 425 (2022) 127995 (https://doi.org/10.1016/j.jhazmat.2021.127995).

[58] M.A. Metwally, M.E. Khalifa, M. Koketsu, Thiocarbohydrazides: Synthesis and reactions, Amer. J. Chem. 2 (2012) 38–51.

[59] M.V. Lopez-Ramon, F. Stoeckli, C. Moreno-Castilla, F. Carrasco-Marin, On the characterization of acidic and basic surface sites on carbons by various techniques, Carbon, 37 (1999) 1215-1221 (https://doi.org/10.1016/s0008-6223(98)00317-0).

[60] Y.S. Ho, G. McKay, Pseudo-second order model for sorption processes, Process Biochem., 34 (1999) 451-465 (https://doi.org/10.1016/S0032-9592(98)00112-5).

[61] J. Crank, The Mathematics of Diffusion, 2nd. ed., Oxford University Press, Oxford, U.K., 1975.

[62] C. Tien, Adsorption Calculations and Modeling, Butterworth-Heinemann, Newton, MA, 1994.

[63] K.H. Chu, Revisiting the Temkin isotherm: Dimensional inconsistency and approximate forms, Ind. Eng. Chem. Res. 60 (2021) 13140–13147, https://doi.org/10.1021/acs.iecr.1c01788.

[64] V. Puccia, M.J. Avena, On the use of the Dubinin-Radushkevich equation to distinguish between physical and chemical adsorption at the solid-water interface, Colloid Interface, Sci. Commun. 41 (2021), 100376, https://doi.org/10.1016/j.colcom.2021.100376.

[65] J. Zhou, D. Wu, D. Guo, Optimization of the production of thiocarbohydrazide using the Taguchi method, J. Chem. Technol. Biotechnol. 85 (2010) 1402–1406, https://doi.org/10.1002/jctb.2446.

[66] E. Mendez, M.F. Cerda, J.S. Gancheff, J. Torres, C. Kremer, J. Castiglioni, M. Kieninger, O.N. Ventura, Tautomeric forms of 2-thiobarbituric acid as studied in the solid, in polar solutions, and on gold nanoparticles, J. Phys. Chem. C 111 (2007) 3369–3383, https://doi.org/10.1021/jp0628176.

[67] M.R. Chierotti, L. Ferrero, N. Garino, R. Gobetto, L. Pellegrino, D. Braga, F. Grepioni, L. Maini, The richest collection of tautomeric polymorphs: The case of 2-thiobarbituric acid, Chem. Eur. J. 16 (2010) 4347–4358, https://doi.org/10.1002/chem.200902485.

[68] M.V. Jovanovic, E.R. Biehl, Substituent and solvent effects on tautomeric equilibria of barbituric acid derivatives and isoterically related compounds, J. Heterocycl. Chem. 24 (1987) 191–204, https://doi.org/10.1002/jhet.5570240136.

[69] C.N.R. Rao, R. Venkataraghavan, The C=S stretching frequency and the "-N-C=S bands" in the infrared, Spectrochim. Acta 18 (1962) 541–547, https://doi.org/10.1016/S0371-1951(62)80164-7.

[70] K. Ramamurthi, G. Madhurambal, B. Ravindran, M. Mariappan, S.C. Mojumdar, The growth and characterization of a metal organic crystal, potassium thiourea thiocyanide, J. Therm. Anal. Calorim. 104 (2011) 943–947, https://doi.org/10.1007/s10973-011-1492-y.

[71] M. Mariappan, G. Madhurambal, B. Ravindran, S.c., Mojumdar, Thermal, FTIR and microhardness studies of bisthiourea-urea single crystal, J. Therm. Anal. Calorim. 104 (2011) 915–921, https://doi.org/10.1007/s10973-011-1293-3.

[72] B.K. Momidi, V. Tekuri, D.R. Trivedi, Multi-signaling thiocarbohydrazide based colorimetric sensors for the selective recognition of heavy metal ions in an aqueous medium, Spectrochim. Acta, Part A 180 (2017) 175–182, https://doi.org/10.1016/j.saa.2017.03.010.

[73] C.A. Téllez Soto, J.M. Ramos, A.C. Costa Junior, L.S. Vieira, J.L. Rangel, L. Raniero, P.P. Fávero, T. Lemma, G.F. Ondar, O. Versiane, A.A. Martin, Surface enhancement Raman scattering of tautomeric thiobarbituric acid. Natural bond orbitals and B3LYP/6-311+G (d, p) assignments of the Fourier Infrared and Fourier Raman Spectra, Spectrochim. Acta, Part A 114 (2013) 475–485, https://doi.org/10.1016/j.saa.2013.05.035.

[74] R. Bhatt, S. Kushwaha, S. Bojja, P. Padmaja, Chitosan–thiobarbituric acid: A superadsorbent for mercury, ACS, Omega 3 (2018) 13183–13194, https://doi.org/10.1021/acsomega.8b01837.

[75] K. Mousapour, S. Hajizadeh, K. Farhadi, Colorimetric speciation analysis of chromium using 2-thiobarbituric acid capped silver nanoparticles, Anal. Methods 12 (2020) 2484–2490, https://doi.org/10.1039/d0ay00160k.

[76] M. Thommes, K. Kaneko, A.V. Neimark, J.P. Olivier, F. Rodriguez-Reinoso, J. Rouquerol, K.S.W. Sing, Physisorption of gases, with special reference to the evaluation of surface area and pore size distribution (IUPAC Technical Report), Pure Appl. Chem. 87 (2015) 1051–1069, https://doi.org/10.1515/pac-2014-1117.

[77] K.S. Siddiqi, S. Khan, S.A.A. Nami, M.M. El-ajaily, Polynuclear transition metal complexes with thiocarbohydrazide and dithiocarbamates, Spectrochim. Acta, Part A 67 (2007) 995–1002, https://doi.org/10.1016/j.saa.2006.09.019.

[78] A.D. Tiwari, A.K. Mishra, S.B. Mishra, B.B. Mamba, B. Maji, S. Bhattacharya, Synthesis and DNA binding studies of Ni(II), Co(II), Cu(II) and Zn(II) metal complexes of N1, N5-bis[pyridine-2-methylene]-thiocarbohydrazone Schiff-base ligand, Spectrochim. Acta, Part A 79 (2011) 1050–1056, https://doi.org/10.1016/j.saa.2011.04.018.

[79] K. Nag, D.S. Joardar, Metal complexes of sulfur–nitrogen chelating agents. V. 2-N-Ethylaminocyclopentene-1-dithiocarboxylic acid complexes of Ni(II), Pd(II), Pt(II), Co(II), Co(III), and Cu(I), Can. J. Chem., 54 (1976) 2827-2831 (https://doi.org/10.1139/v76-400).

[80] A. Werner, A. Rieger, M. Mosch, R. Haseneder, J.-U. Repke, Nanofiltration of indium and germanium ions in aqueous solutions: Influence of pH and charge on retention and membrane flux, Sep. Purif. Technol. 194 (2018) 319–328, https://doi.org/10.1016/j.seppur.2017.11.006.

[81] S.A. Wood, I.M. Samson, The aqueous geochemistry of gallium, germanium, indium and scandium, Ore Geol. Rev. 28 (2006) 57–102, https://doi.org/10.1016/j.oregeorev.2003.06.002.

[82] M. Li, X. Meng, K. Huang, J. Feng, S. Jiang, A novel composite adsorbent for the separation and recovery of indium from aqueous solutions, Hydrometallurgy 186 (2019) 73–82, https://doi.org/10.1016/j.hydromet.2019.04.003.

[83] D.S.P. Franco, J. Vieillard, N.P.G. Salau, G.L. Dotto, Interpretations on the mechanism of In(III) adsorption onto chitosan and chitin: A mass transfer model approach, J. Mol. Liq. 304 (2020), https://doi.org/10.1016/j.molliq.2020.112758.

[84] M.A. Hubbe, S. Azizian, S. Douven, Implications of apparent pseudo-second-order adsorption kinetics onto cellulosic materials: A review, BioResources 14 (2019) 7582–7626.

[85] K. Avchukir, B.D. Burkitbayeva, A.M. Argimbayeva, G.S. Rakhymbay, G. S. Beisenova, M.K. Nauryzbayev, The kinetics of indium electroreduction from chloride solutions, Russ. J. Electrochem. 54 (2018) 1096–1103, https://doi.org/10.1134/S1023193518120042.

[86] M.H. Tehrani, E. Companys, A. Dago, J. Puy, J. Galceran, Free indium concentration determined with AGNES, Sci. Total Environ. 612 (2018) 269–275, https://doi.org/10.1016/j.scitotenv.2017.08.200.

[87] S. Kariuki, H.D. Dewald, Polarographic determination of diffusion coefficient values of In(III) in potassium chloride and nitrate supporting electrolytes, Talanta 44 (1997) 1765–1771, https://doi.org/10.1016/S0039-9140(97)00046-5.

[88] H.N. Tran, E.C. Lima, R.-S. Juang, J.-C. Bollinger, H.-P. Chao, Thermodynamic parameters of liquid–phase adsorption process calculated from different equilibrium constants related to adsorption isotherms: A comparison study, J. Environ Chem. Eng. 9 (2021), 106674, https://doi.org/10.1016/j.jece.2021.106674.

[89] H.M. Li, J.S. Liu, X.Z. Gao, C. Liu, L. Guo, S.X. Zhang, X.Y. Liu, C.P. Liu, Adsorption behavior of indium(III) on modified solvent impregnated resins (MSIRs) containing sec-octylphenoxy acetic acid, Hydrometallurgy 121 (2012) 60–67, https://doi.org/10.1016/j.hydromet.2012.04.005.

[90] K. Zhang, Y. Wu, W. Wang, B. Li, Y. Zhang, T. Zuo, Recycling indium from waste LCDs: A review, Resour. Conserv. Recycl. 104 (2015) 276–290, https://doi.org/10.1016/j.resconrec.2015.07.015.

[91] K.L. Timofeev, G.I. Maltsev, A.V. Usol'tsev, S.S. Naboichenko, Sorption technology of recovery of indium from solutions of zinc production, Russ. J. Non-Ferrous Met. 58 (2017) 225–230, https://doi.org/10.3103/s1067821217030191.

[92] H. Tokuyama, T. Yoshida, L. He, Preparation of novel emulsion gel adsorbents and their adsorption properties for heavy-metal ions, Ind. Eng. Chem. Res. 50 (2011) 10270–10277, https://doi.org/10.1021/ie201179n.

[93] E. Nieboer, D.H.S. Richardson, The replacement of the non-descript therm heavy-metals by a biologically and chemically significant classification of metal-ions, Environ. Pollut. Series B 1 (1980) 3–26, https://doi.org/10.1016/0143-148x(80)90017-8.

[94] R.G. Pearson, Acids and bases, Science (New York, N.Y.), 151 (1966) 172-177 (https://doi.org/10.1126/science.151.3707.172).

[95] T.-N. Kwon, C. Jeon, Selective adsorption for indium(III) from industrial wastewater using chemically modified sawdust, Korean J. Chem. Eng. 29 (2012) 1730–1734, https://doi.org/10.1007/s11814-012-0069-1.

[96] M. Li, X. Meng, X. Liang, J. Yuan, X. Hu, Z. Wu, X. Yuan, A novel In(III) ion-imprinted polymer (IIP) for selective extraction of In(III) ions from aqueous solutions, Hydrometallurgy 176 (2018) 243–252, https://doi.org/10.1016/j.hydromet.2018.02.006.

[97] R.S. Marinho, C.N. da Silva, J.C. Afonso, J. da Cunha, Recovery of platinum, tin and indium from spent catalysts in chloride medium using strong basic anion exchange resins, J. Hazard. Mater. 192 (2011) 1155–1160, https://doi.org/10.1016/j.jhazmat.2011.06.021.

[98] M.A. Zahran, K.F. Mahmoud, M.A. Mahdy, A.M. Abd El-Hamid, Leaching of gallium from gaiter granite, eastern desert, Egypt, Isot. Radiat. Res. 39 (2006) 115–126.